CRITERIA AND TESTS FOR COLD HEADABILITY

by

Yasmine Sarruf

A Thesis Submitted to the Faculty of Graduate Studies and Research in Partial Fulfillment of the Requirements for the Degree of Master of Engineering

Department of Mining and Metallurgical Engineering
McGill University
Montreal, Canada

0-612-70250-2

ABSTRACT

It is quite difficult to quantitatively define the ability of a material to be cold forged. The limit of the forming process is governed by a complicated interplay of such factors as material microstructure, rate of deformation, tool and workpiece geometry and the friction at the interface of the workpiece and tool.

The success of a cold forming process is primarily determined by the formability of the stock material. Consistent product quality and increase in productivity requires parts to be plastically deformed without failure. Expensive downtime, tooling damage and material waste are often the consequences of material failure during loading. A means of assessing formability is, therefore, clearly required.

A revised upset test is examined, seeking to represent the actual cold heading process and to minimize the effect of test specific factors, such as changing friction at the die-workpiece interface. It is designed to be easily used by industry, requiring minimal sample preparation and the use of a simple and reliable testing device. Preliminary tests are performed and the limitations of this test are investigated. Possibilities for future improvements are considered.

RÉSUMÉ

Il est dificile de définir en terme quantitatif la capacité de forger un matériel à froid. La limite du processus de formation est établie par une intéraction complexe de tels facteurs comme la micro-structure des matériaux, le taux de déformation, la géométrie de l'outil et des pièces de travail ainsi que la friction à l'interface de cette pièce.

Le succès du procéssus de formation à froid est essentiellement défini par le façonnement des matériaux en réserve. La qualité constante du produit et l'augmentation de la productivité demandent que des pièces soient déformées sans faillite. L'inactivité coûteuse, l'endommagement des outils, et le gaspillage des matériaux sont souvent les conséquences de la faillite des matériaux durant chargement. Un moyen de mesurer la formation à froid est donc clairement requis.

La révision d'un test renversé est examiné tout en cherchant à répresenter le procéssus véritable de formation à froid ainsi que de minimiser l'effet des facteurs spécifiques du test, comme le changement de friction entre la matrice et la pièce de travail. Le test, désigné pour être utilisé par industrie, exige la préparation avec un nombre minime d'échantillons, ainsi que l'utilisation d'un instrument de test simple et fiable. Les tests préliminaires sont complétés et les limitations de ce test sont examinés. Les possibilités pour une amélioration dans le futur sont examinées.

ACKNOWLEDGEMENTS

I would like to express my sincere gratitude to my thesis supervisor, Prof. J. J. Jonas, for his continual support and guidance throughout the course of this work. His knowledge and assistance were of great value. Research Associate Bao-Hong Cao's insight and advice were always welcome and helpful. I wish to also very much thank Ivaco Rolling Mills for their support of this work, in particular, Michel Hone and Nick Nickoletopoulos.

I would like to thank Lorraine Mello for her administrative help and friendly disposition, Edwin Fernandez for his laboratory expertise and "international lunches", Helen Campbell for her assistance with the SEM and Monique Riendeau for her help with the chemical analysis.

I am also very grateful to my classmates, some of whom became close friends. They filled my years at McGill with great memories and ensured that those times will not be forgotten. Finally, I would like to thank my family, whose support and patience with me are very much appreciated.

TABLE OF CONTENTS

LIST OF FIGURES

CHAPTER II

CHAPTER III

CHAPTER IV

LIST OF TABLES

CHAPTER I

INTRODUCTION

It is quite difficult to quantitatively define the ability of a material to be cold forged. The limit of the forming process is governed by a complicated interplay of such factors as material microstructure, rate of deformation, tool and workpiece geometry and the friction at the interface of the workpiece and tool.[1]

The success of a cold forming process is primarily determined by the formability of the stock material. Consistent product quality and increase in productivity require parts to be plastically deformed without failure. Expensive press downtime, tooling damage and material waste are often the consequences of material failure during loading. A means of assessing formability is, therefore, clearly required.

Traditionally, cold headability has been evaluated by means of an upset test. While this laboratory test does permit a comparison to be made between various materials, it possesses several disadvantages in terms of accurately simulating the cold heading process and yielding reproducible results. Although the upset test is capable of examining the suitability of a material for heading, it is intended mainly as a means of revealing internal and external defects.[2,3] Thus, efforts have been made to devise more reliable testing methods of assessing headability.

It is the aim of this work, after examining several of these recent developments,[4,5,6] to design a revised upset test and to perform headability tests on materials of interest. This study will attempt to take into account all factors that could affect the test results, as well as define the test conditions comprehensively and accurately. The results will be analyzed and suggestions for future improvements made.

CHAPTER II

LITERATURE REVIEW

2.1 CONVENTIONAL PROCEDURES FOR THE MANUFACTURE OF COLD HEADING QUALITY STEEL WIRE

The production of cold heading quality (CHQ) steel wire demands fairly sophisticated processing steps, shown in Figure 2.1, that must be performed under tight control. The final product should possess an essentially defect-free surface, a ductile microstructure and a coating with superior lubricating properties.[3]

CHQ steel wire is manufactured from a high quality hot rolled rod of suitable chemistry. Surface scale is then removed from the rod and it is coated to prevent rusting and to provide a surface that readily picks up drawing lubricants. The rod is then cold drawn to size and heat treated to yield a ductile spheroidized microstructure. The wire is cleaned, coated with phosphate and lime, inspected and shipped. Depending on the customer requirements, some CHQ wire is redrawn after coating.[3] While this is the usual sequence of events involved in the manufacturing of CHQ steel wire, there are certainly variations that exist, depending on the steel mill.

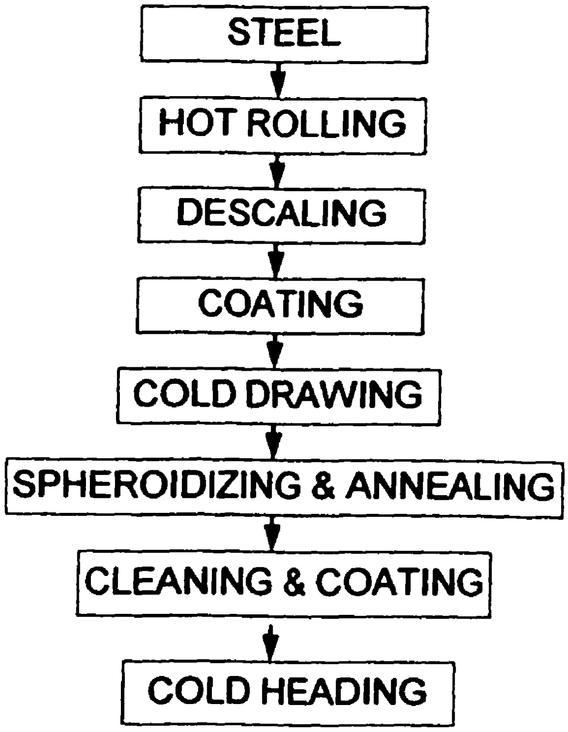

Figure 2.1 - Conventional procedure for the manufacture of CHQ steel wire[3]

2.2 THE COLD HEADING PROCESS

Cold heading is a cold forging process whereby the force developed by one or more blows of a heading tool is used to upset the metal in a portion of a wire blank in order to form a section of a different contour. The cold heading of an unsupported wire on a horizontal machine is illustrated in Figure 2.2.[7] The cross-sectional area of the initial material is increased as the height of the workpiece is decreased. The process requires very high strain rates, usually greater than $10^2\ s^{-1}$.[4]

There are several advantages of the cold heading process over machining of the same parts. These include little waste material, increased tensile strength from cold working and controlled grain growth. Aside from its main use for the production of heads on rivets or on blanks for threaded fasteners, many other shapes can be successfully and economically formed by cold heading.[7]

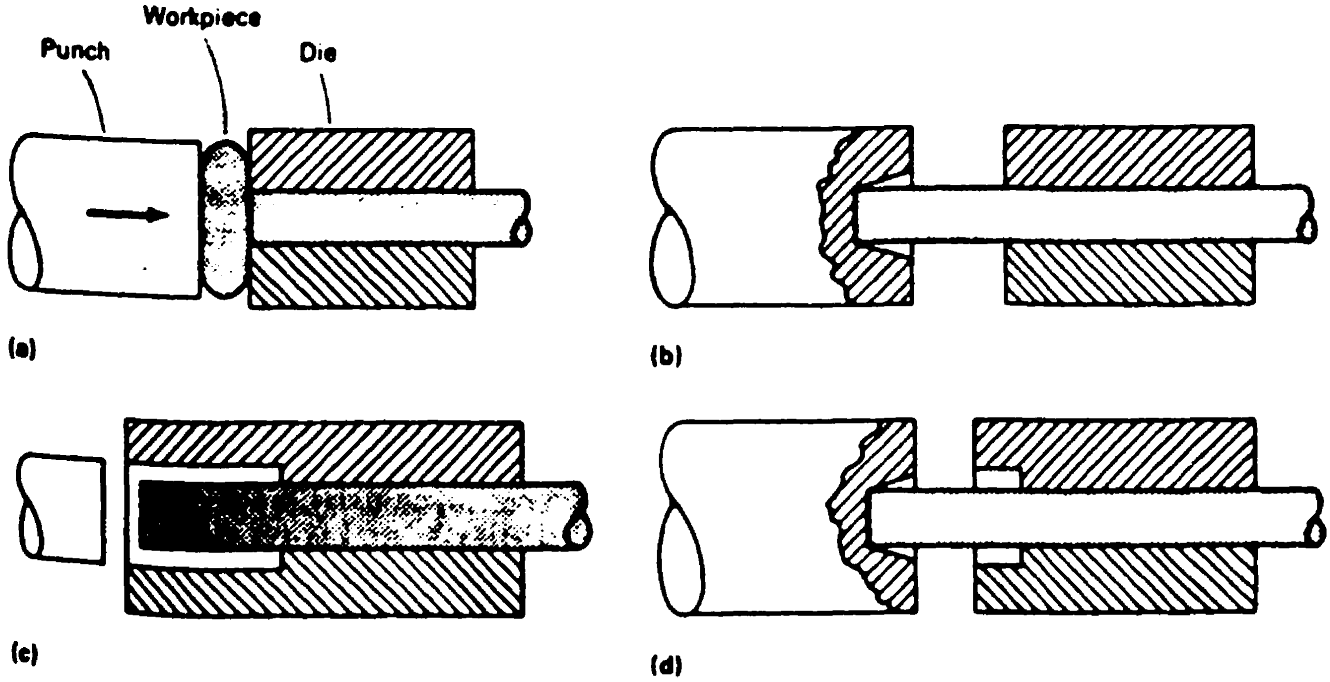

Figure 2.2 - Schematics of the cold heading of an unsupported bar in a horizontal machine[7]
a) head formed between punch and die b) head formed in punch
c) head formed in die d) head formed in punch and die

2.3 QUALITY REQUIREMENTS FOR CHQ STEEL WIRE

Cold headability is the ability of a cylindrical piece of material to be shaped into the head of a bolt, screw or other cold formed part without cracking at high strain rates.[3] In order to achieve a satisfactory level of cold headability, there are certain stringent quality requirements that the steel wire must meet. It is generally agreed upon that better cold headability can be achieved with steels of lower strength and strain hardening exponent (n).[4] The cold heading material must be sufficiently soft and ductile not to resist the upsetting operation.[8]

2.3.1 SURFACE QUALITY

Surface quality is of great importance during the cold heading process. Surface defects occur mostly as seams, cracks, shells and rolling laps. They are characterized in terms of their depth, width and length. Care must be taken to minimize surface defects throughout the production process, as they may arise at any stage, from the melt shop to the finishing mills.[8] If allowed to occur, surface defects will, rather than act as stress raisers, act as strain discontinuities and alter the strain path.[5]

2.3.2 INTERNAL SOUNDNESS

Internal soundness also effects the cold headability of steel wire. The quantity, size and nature of internal defects that can be tolerated is dependent upon the particular type of heading process. In the case of excessive amounts of nonmetallic inclusions or internal segregation, internal shear failures may result due to the nature of metal flow during the cold heading process. Failure can also result during upsetting due to a reduction in the ability of the metal to flow through variations in grain size.[8]

2.3.3 MICROSTRUCTURE

In terms of microstructure, superior ductility in steel is obtained when the carbides are present in spheroidized form.[8] Ductile fracture occurs through the stages of void nucleation, growth and coalescence. As spheroidization results in an increased strain requirement for void nucleation, the cold headability of the steel is increased through the presence of such a microstructure.

2.3.4 ALLOYING ELEMENTS

Alloy additions also play a role in determining cold headability. Studies have shown that the ferrite soluble elements phosphorus, manganese, silicon and nickel increase the deformation resistance of spheroidized and annealed steels.[9] Molybdenum and chromium appear to be concentrated in the carbide phase and contribute little to the deformation resistance. Therefore, it is desirable to produce steels with the ferrite strengthening elements present at the lowest practical limits for tonnage steel making and with molybdenum and chromium added for hardenability. Chromium-molybdenum steels low in manganese and nickel also possess the added advantage of exhibiting a higher than normal A_{c1} temperature for a given carbon content. Thus, they are readily spheroidized prior to forming and easily subcritically annealed when required between forming operations. Tests have also shown that the microstructure, tensile properties and cold forgeability of spheroidized medium carbon steels are not negatively affected by the addition of Cu, Sn and Sb at levels of less than 0.5%, 0.1% and 0.1%, respectively.[10] It is rather the inclusion size distribution that mainly determines the cold forgeability of such steels.

2.3.5 PREDRAWING

The effect of a prestrain on the formability of cold heading quality steel is of considerable consequence. Wire drawing after process annealing can increase ductility in subsequent heading operations. However, the degree of cold heading after drawing generally varies inversely with the tensile reduction in area. Thus, tensile ductility parameters, i.e., elongation and reduction of area, are not necessarily reflective of cold heading performance.[5,11,12] A predrawing reduction of about 35% through dies of angles ranging from 12° to 20° has been found to result in a significant increase in the cold headability.[13] It has been suggested that this improvement in ductility is related to a reduction in the potential for strain aging.[5]

2.4 CONVENTIONAL METHODS FOR ASSESSING COLD HEADABILITY

There are several tests that are presently used to assess the characteristics of CHQ wire. These include diameter measurements in order to ensure that dimensional tolerances are being met. In addition, tensile and hardness tests are often performed to evaluate mechanical properties and ductility through the determination of values such as the ultimate tensile strength, reduction of area and percentage elongation. A common method for revealing surface defects is an acid pickle test. This allows for visual inspection of the sample wire followed by metallographic examination to determine the origin and depth of the defects.[3]

In terms of establishing the potential for fracture during cold heading, i.e., the cold headability, the combination of a workability test with a fracture criterion is required.

The former determines the ductility of the material under normal conditions, while the latter extends this finding to the particular stress and strain conditions of a specific cold heading process. Thus, it is important to ensure that the workability test simulates the type of fracture that actually occurs during cold heading.[14] While the upset test is frequently used as a means of revealing internal and external defects, it has the potential of also evaluating the headability. The upset test involves the longitudinal compression of a short sample of wire between platens and observing the reduction in height at which cracking of the sample commences.[3]

The presence of friction at the die surfaces during an upset test causes the shape of the specimen to become bulged or barreled. As spread is restricted at the end faces of the specimen, little or no deformation occurs here. Rather, all the expansion occurs around the circumference of the central plane. The severity of the bulged cylindrical surface increases with increasing friction and decreasing specimen aspect (height to diameter) ratio. It is the circumferential strain associated with the bulging surface that renders the upset test an appropriate workability test.[14]

Strain measurements are made by measuring the spacing between grid marks that are placed on the equatorial surface, illustrated in Figure 2.3, according to the following relationships:

$$\text{axial strain} : \varepsilon_z = \ln(\frac{h}{h_o})$$

$$\text{hoop strain}: \varepsilon_\theta = \ln(\frac{W}{W_o}) \quad \text{or} \quad \ln(\frac{D}{D_o})$$

where h_o and h are the initial and final gauge heights, respectively, W_o and W are the initial and final gauge widths, respectively, and D_o and D are the initial and final diameters, respectively.[14]

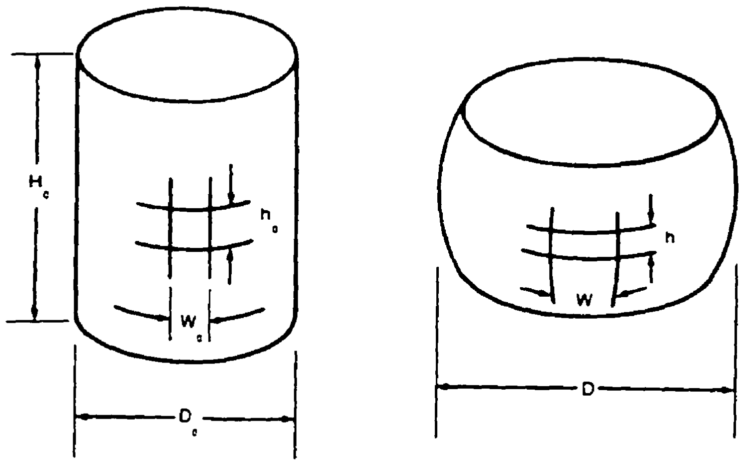

Figure 2.3 - Grids for strain measurements on upset cylinders[14]

The strains associated with the bulging free surface are affected by the aspect ratio as well as the friction conditions.[14] The upper limit on the aspect ratio is set at 2 to avoid buckling, while the lower limit is based on a suitable height for the use of grid marks. The usual range of aspect ratios is 0.75 to 1.75. Friction conditions can be altered through the use of various lubricants and dies with polished, ground and intermediate surface conditions. The end faces of specimens are usually polished to avoid lubricant entrapment.

A different combination of axial compressive strain and circumferential tensile strain at the free surface of the specimen is obtained from each combination of friction conditions and aspect ratio. The large range of possible conditions allows the effects of changes in stress and strain states on the occurrence of fracture to be determined. Thus, by performing numerous tests, each combination of surface strains at fracture will determine a point on the fracture limit line, as illustrated in Figure 2.4. Results from homogeneous (frictionless) cylindrical compression tests fit a straight line with a slope of one half regardless of the material.[15] The vertical intercept is dependent upon the material being tested.

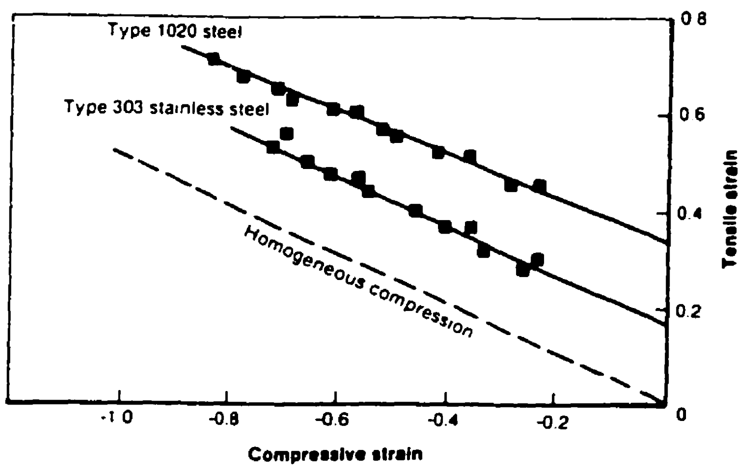

Figure 2.4 - Fracture loci in cylindrical upset test specimens of two materials[14]

In addition to determining the fracture strains, the free surface strains during the actual deformation process must also be evaluated. Though strain paths are material independent, they are process and geometry dependent.[16] Thus, strain paths for various combinations of friction conditions and aspect ratios can be constructed. As seen in Figure 2.5, the tensile strain is equal to one half the compressive strain during the homogeneous compression of a cylindrical specimen.[14,17,18] As the friction is increased, the strain path slope becomes steeper due to a decrease in the compressive strain and a growth in the tensile strain. For a given value of friction, the strain path slope will increase slightly as the aspect ratio decreases.

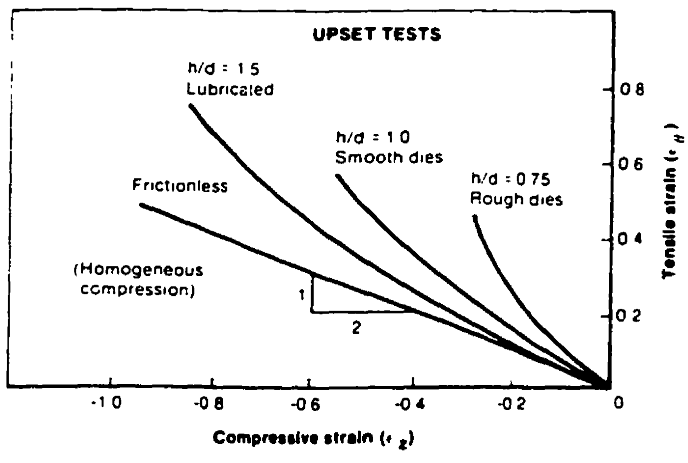

Figure 2.5 - Strain paths in upset test specimens[14]

A forming limit diagram can then be produced by combining Figures 2.4 and 2.5. Figure 2.6 incorporates the effect of the material in the fracture limit line, as well as the process influence through alterations in strain path as a result of changes in friction and specimen geometry.

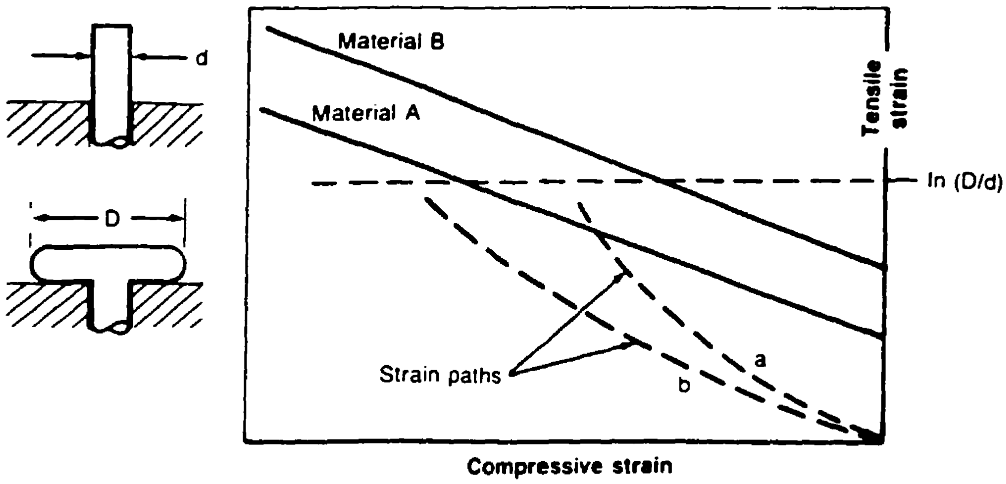

Figure 2.6 - Forming limit diagram - comparison of strain paths and fracture locus lines[14]

Thus, a valid measurement of workability limits due to surface fracture in bulk deformation is possible through upset tests due to the similarities in the deformation gradients. Cracks occur as a result of surface strain states, a critical component of the upset test. The surface material is backed up by the interior material, which experiences less tensile deformation. Processes such as bolt heading undergo a similar deformation pattern. The validity of this method has been confirmed through the recent successful application of workability limits obtained using the upset test.[14]

2.5 DISADVANTAGES OF CONVENTIONAL METHODS FOR ASSESSING COLD HEADABILITY

There are several drawbacks to the standard tests that are often used to determine cold headability. The tensile test employs much lower strain rates ($< 10^{-1}\ s^{-1}$) than those encountered in the actual cold heading process ($> 10^{2}\ s^{-1}$). While the upset test does provide certain useful information, there are several factors that diminish its ability to accurately simulate the cold heading process. Firstly, similar to the tensile test, it generates significantly lower strain rates than those involved in heading. As well, the method by which failure is determined, i.e., the appearance of a surface crack, is visual and quite subjective. Furthermore, the friction conditions associated with the upset test are not similar to those in heading. Finally, it is not possible, through the upset test, to produce a significant amount of data that can be used to quantitatively rate headability.[3]

2.6 RECENT DEVELOPMENTS REGARDING METHODS FOR ASSESSING COLD HEADABILITY

2.6.1 HEADABILITY IMPACT TEST

In an attempt to address the shortcomings of conventional procedures for assessing cold headability, several new methods have been explored. One such method is the headability impact test.[3] It is based on an impact test philosophy, whereby the material is deformed to failure and the data from the deformation event are analyzed. An instrumented impact tester possessing production header dies and punches deforms a wire specimen to failure. A record of the force displacement curve of the impact event is obtained, the failure point identified and data generated for calculation of a headability rating.

As seen in Figure 2.7, the specimen is completely supported so as to avoid buckling. The dies and spacer are held in a die case. The punch pin is forced down by the impact tester ram and then pushes the wire out of the upper die into the cavity forming the head. The high speed instrumented impact tester is capable of providing 500 joules of energy at a maximum initial velocity of 7 m/s. To ensure bulk failure of the material, more than four diameters of wire are usually required in the head. This promotes the preferred mode of failure for assessing cold headability, illustrated in Figure 2.8. The 45^0 shear crack indicates that the plastic deformation limit of the material has been reached. Surface defects are revealed through cracks parallel to the longitudinal axis.[3]

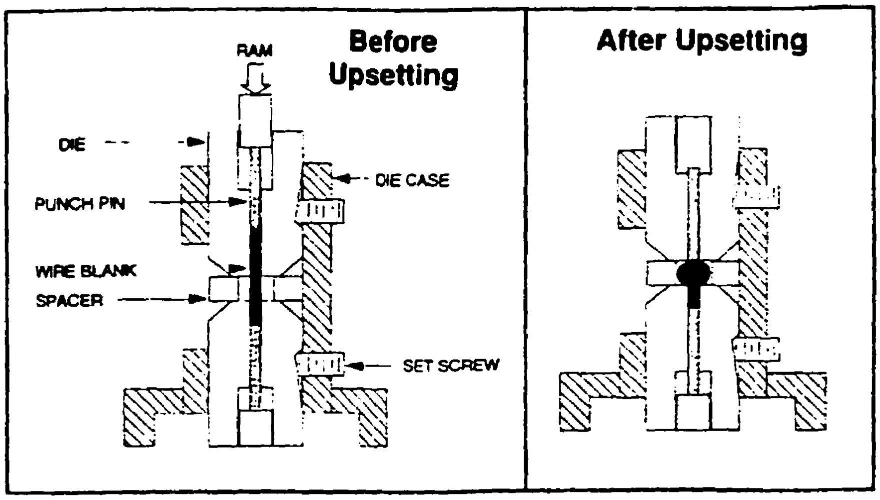

Figure 2.7 - Headability test tooling[3]

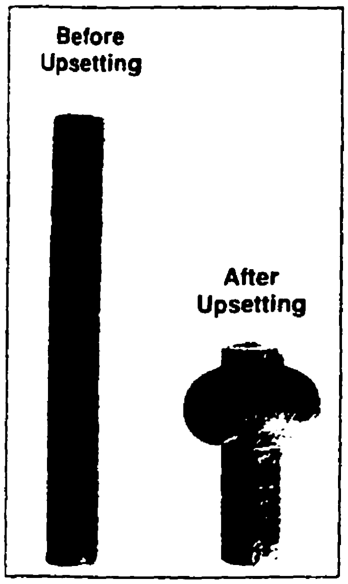

Figure 2.8 - Cracked headability test specimen[3]

In order to calculate a headability rating, certain parameters are obtained from the force-displacement curve, shown in Figure 2.9. The ductility of the sample can be found by determining the displacement to the point of cracking on the curve. The energy to failure is equal to the area under the curve up to the failure point. The work hardening rate is determined through the maximum slope on the curve between the yield point and the peak load. Finally, the peak load is simply the maximum force experienced during the deformation process. It was found that by expressing each of these four parameters as a dimensionless number (shown below), simple multiplication of the factors displayed the expected trends of a headability rating number. One such trend, displayed in Figure 2.10, is the clear decrease in headability as the carbon equivalent is increased.[3]

$$D = \text{DUCTILITY FACTOR} = \frac{\text{initial length} - \text{final length}}{\text{wire diameter}}$$

$$P = \text{PEAK LOAD FACTOR} = \frac{\text{reference peak load} (= 0.75 \text{ punch pin failure load})}{\text{test peak load}}$$

$$N = \text{HARDENING FACTOR} = \frac{\text{reference hardening rate} (= \text{max. value for Grade 1022})}{\text{test hardening rate}}$$

$$E = \text{TOUGHNESS FACTOR} = \frac{\text{reference energy to break (for Grade 1022)}}{\text{test energy to break}}$$

where headability rating number = D x P x N x E

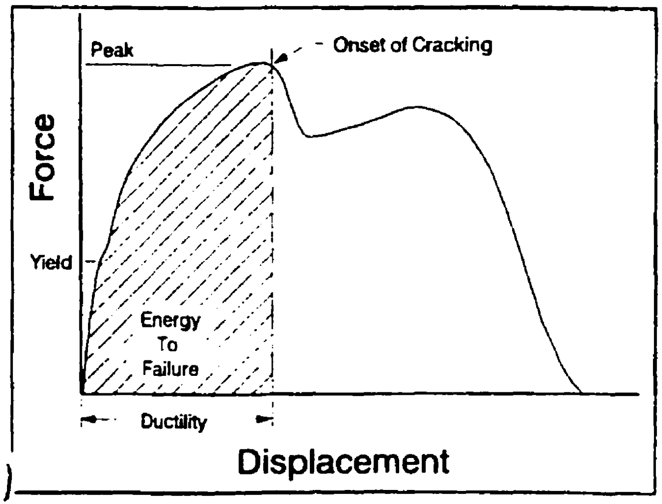

Figure 2.9 – Typical force-displacement curve during deformation[3]

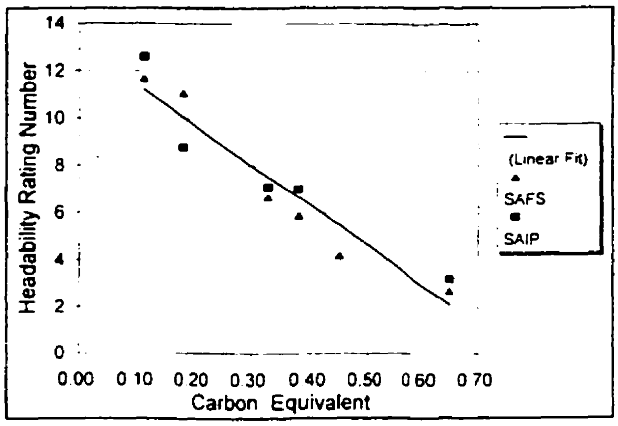

Figure 2.10 - Relationship between carbon equivalent and headability rating # [3]

While the headability impact tester appeared to be a useful means of measuring cold heading parameters in the laboratory, it is no longer in operation. It was felt that similar results were obtainable through more conventional upset test methods.

2.6.2 SPLIT HOPKINSON PRESSURE BAR TEST

Another approach taken to minimize the lack of accuracy present in traditional means of assessing cold headability was to investigate the possibility of utilizing a very high strain rate compression tester, known as the split Hopkinson pressure bar tester.[4]

As illustrated in Figure 2.11, this apparatus consists of two alloy steel bars with strain gauges between which the specimen is mounted. A third alloy striker is propelled by an air pressure gun and provides the impact. An elastic compressive wave is generated within the incident bar upon impact and the time dependent strain is measured by means of the strain gauge attached to the incident bar. The wave is partially reflected and partially transmitted into the specimen. The reflected portion, which travels back along the incident pressure bar, is in the form of a tensile wave and the strain is again measured by the strain gauge attached to the incident bar. The strain gauge attached to the transmitted bar measures the transmitted portion in the form of a compressive wave. The strain rate within the specimen when deformed uniformly is proportional to the amplitude of the reflected wave. Similarly, the stress produced in the specimen is proportional to the amplitude of the transmitted wave. A digital oscilloscope records these two signals and the reflected wave is integrated to yield the strain. The combined signal of the reflected and transmitted waves produces a dynamic stress-strain curve via a developed computer program.

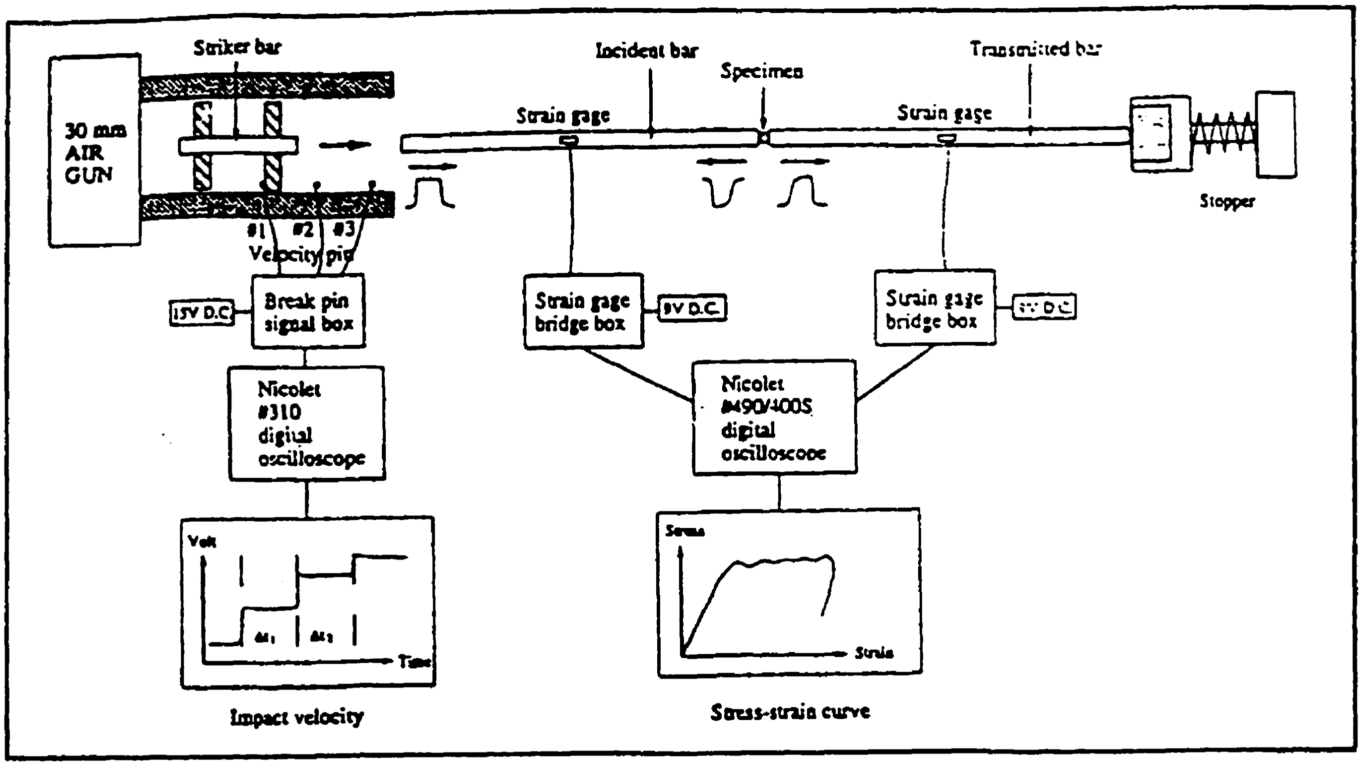

Figure 2.11 - Schematic diagram of the split Hopkinson pressure bar tester[4]

It was found that the split Hopkinson pressure bar is a useful means of assessing the dynamic deformation resistance during the cold heading process. Results obtained using this method agreed with those from traditional tests.[4] However, this equipment is not without its weaknesses. The major limitation is the difficulty involved in ensuring that the specimen undergoes uniform deformation.[19] As well, the equipment requires considerable expertise to operate properly and requires a significant capital investment.

2.6.3 INSTRUMENTED COLD HEADING MACHINE TEST

Yet another approach studied was the use of a full scale production cold heading machine.[5] This method is thought to overcome three experimental difficulties encountered with conventional methods: the uncertainty in deformation path, the inaccurate strain rate and the great effort necessary for sample preparation and testing of single specimens to evaluate variations that may be present within a rod coil. Thus, a commercial cold heading machine can be a means of providing a more useful assessment of formability and ductility, allowing sources of variation in behaviour to be examined with a view to optimizing composition and processing.

Specialist part forming cold heading machines are available for producing specific parts, such as bolts. Should further refinements be made to such a machine, a relatively high level of versatility can be obtained at a lower cost. Such a compromise between a single blow and a multistage machine was chosen to be studied by the researchers of reference 5, namely one capable of delivering one blow on the first die and two blows on the second die.

The machine selected by these coworkers was a Greenbat No. 3 Mk. 3 advanced parts former, depicted in Figure 2.12. It has a maximum input diameter of 13 mm, allowing the heading of both rod and wire of the size range usually delivered by rod mills. It has a heading load of 85 tons and a 40 horsepower motor. Wire is taken from the bollard, passed through the straightening rolls and then the feed rolls, as illustrated in Figure 2.13. These index the wire to the cold forging area of the machine, shown in Figure 2.14, where it is cut off, formed and discharged onto a conveyor belt.[5]

A schematic of the punch and block arrangement is provided in Figure 2.15. Once the wire has been fed and cut off, it is transferred by the transfer fingers to the front of the extrusion die. The first extrusion blow then occurs when the punch block, which delivers blows when in one of the extreme vertical positions, is in its lower position. As the transfer fingers withdraw, the blank is pressed by the punch into the extrusion die. The extruded blank is pushed from the extrusion die by the ejector pin into the transfer punch. The blank then becomes aligned with the heading die as it moves to the lower position. The transfer punch delivers the first heading blow. The position of the heading die profile and the head die ejector pin dictates the extent of upsetting. The punch block first moves to align the final punch with the heading die and then moves forward to strike the final blow. The final punch withdraws and the heading die ejector pin ejects the blank, which is then directed by a jet of compressed air.[5]

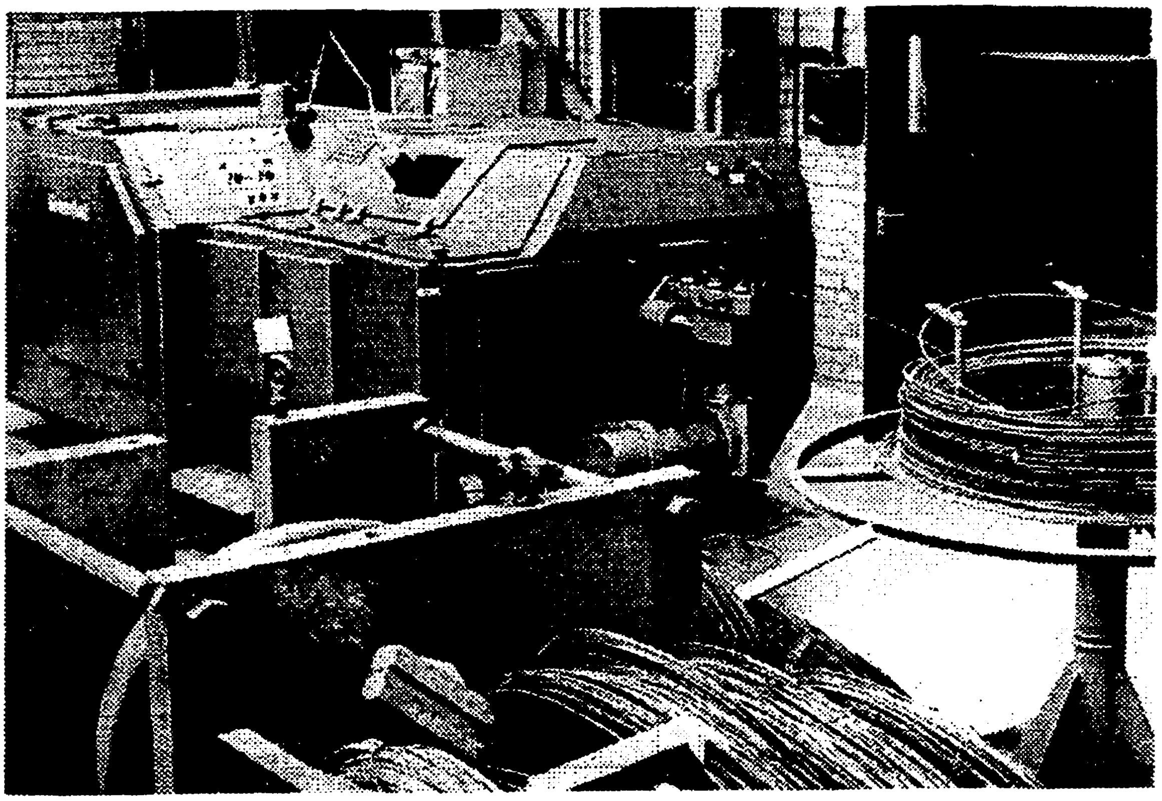

Figure 2.12 - Greenbat cold forging machine[5]

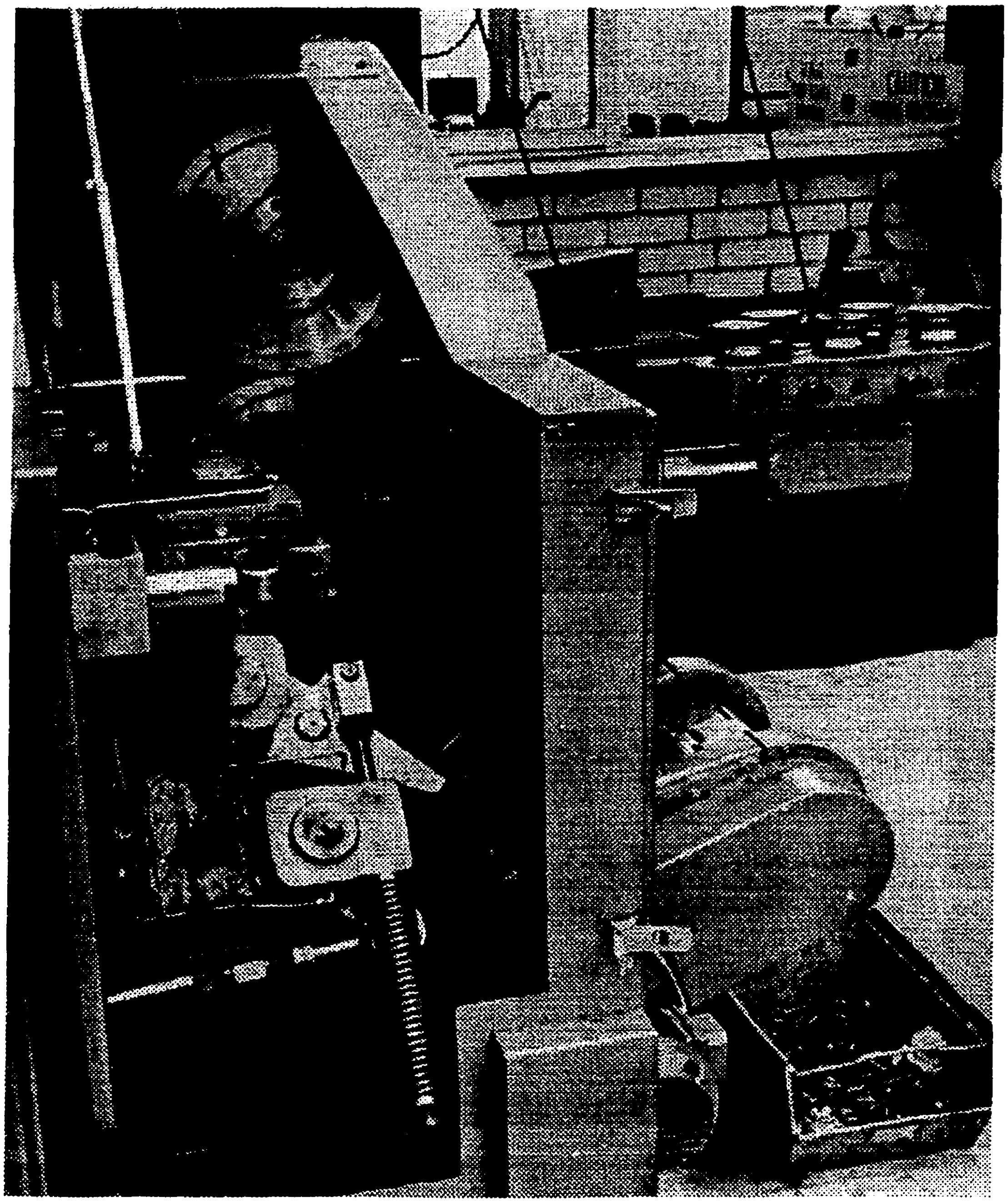

Figure 2.13 - Feed and straightening rolls[5]

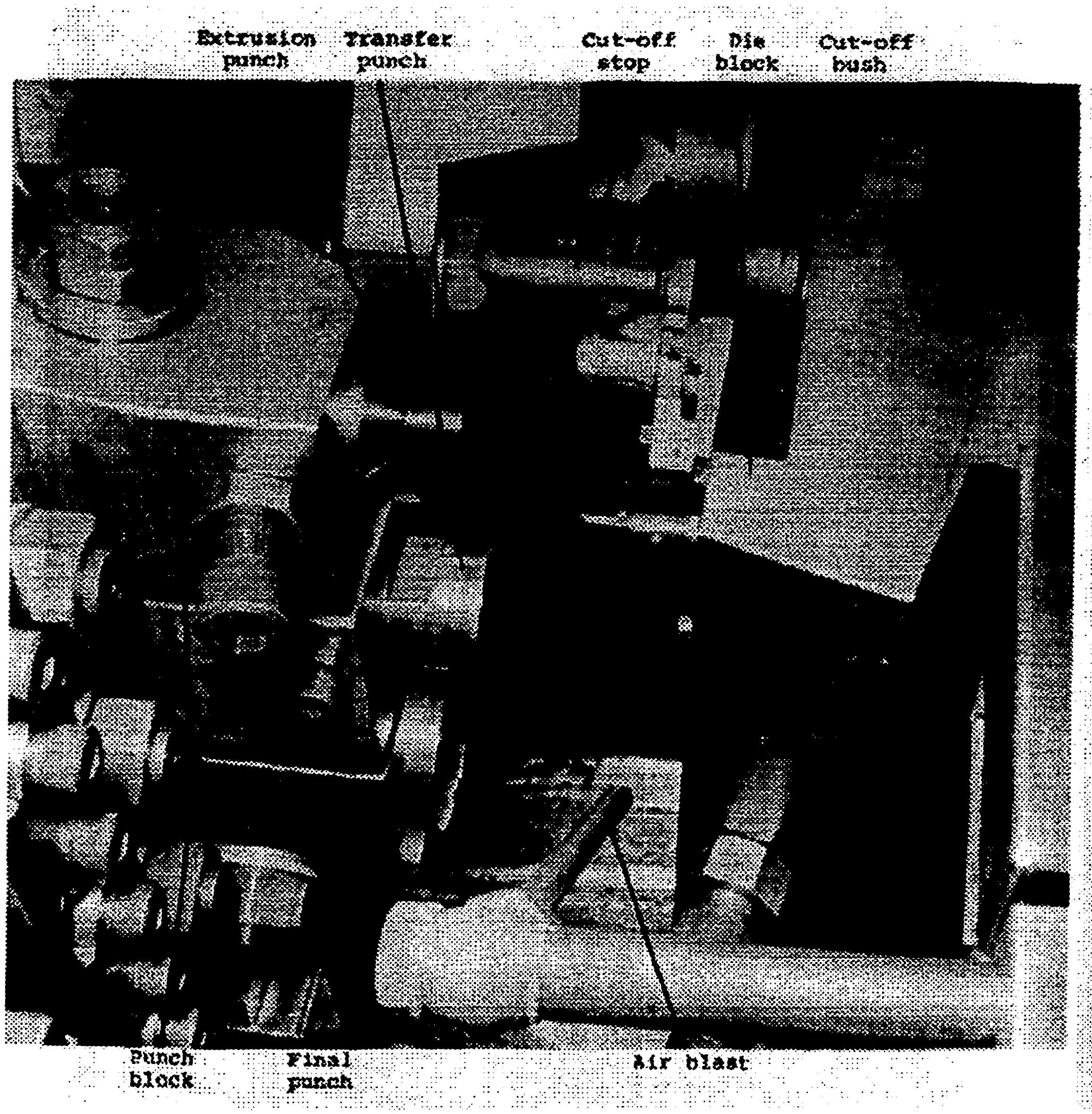

Figure 2.14 - Cold forging area of the machine[5]

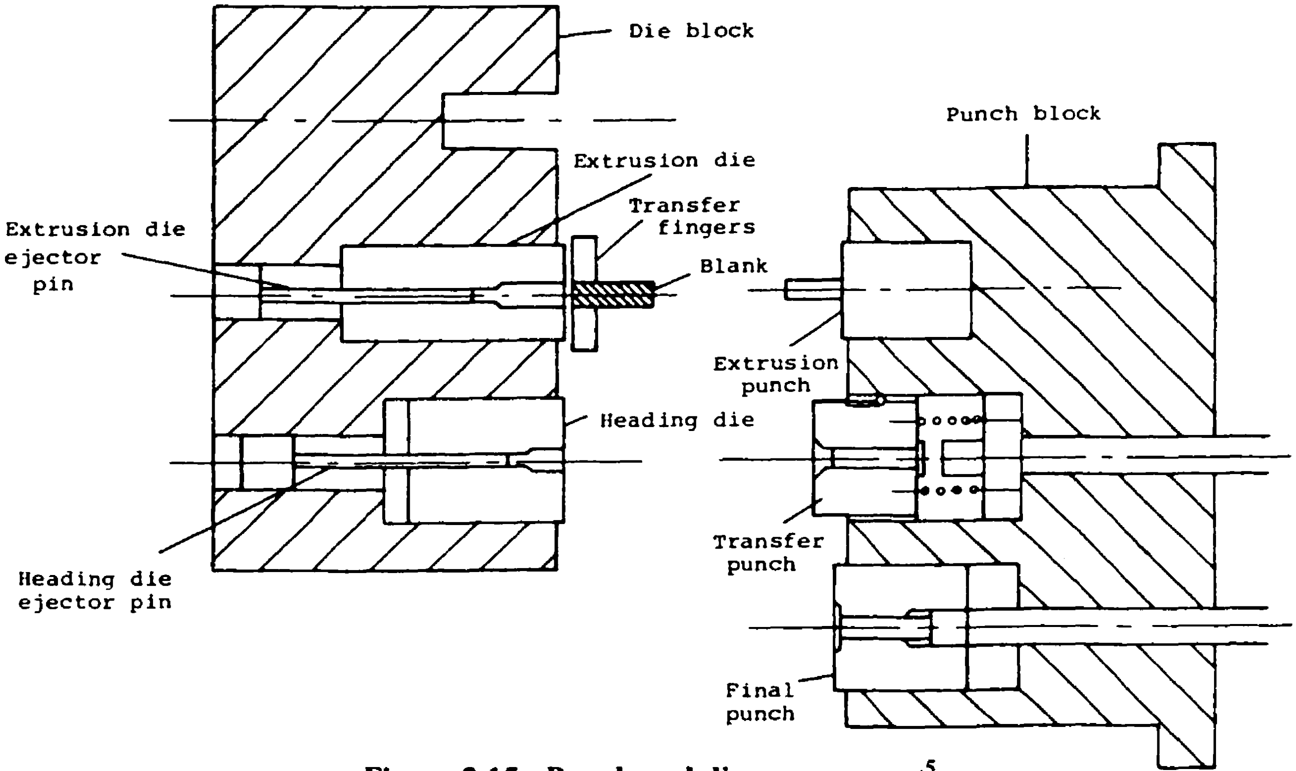

Figure 2.15 - Punch and die arrangement[5]

In terms of instrumentation, the first and second stage heading punches are monitored with load cells and strain gauges. The transfer punch load cell is located near the spacer block in the transfer punch holder. The final punch load cell is positioned behind the final punch, between which a spacer of the appropriate thickness is placed.

In order to obtain energy curves, the punch displacement must be monitored dynamically during the load measurements. Therefore, a striker plate is placed on the punch plate to allow a transducer holding jig, situated on the die block, to hold standard linear displacement transducers that operate during the forming operation. Displacement measurements are obtained through the use of an REP Instruments linear voltage displacement transformer, which is attached to a phase sensitive detector to obtain a linearly proportional voltage output signal. In order that force-displacement curves be displayed directly, a digital transient recorder is used to obtain signals of both the force and displacement signals. These are then replayed into an X-Y flat bed recorder at slow speed. The signals can also be replayed onto a paper chart recorder to display their variation with time.[5] Some typical force-displacement curves for both single and double blow heading tests are shown in Figures 2.16 a) and b), respectively. As can be seen, various heading severities were chosen to represent a light, moderate and severe upset. In addition, the double blow heading tests involved two, three and four wire diameters in the head volume.

The instrumented cold heading machine allows for the direct study of variations in cold heading behaviour. The composition and processing conditions can then be altered accordingly in order to increase the efficiency of cold heading operations.

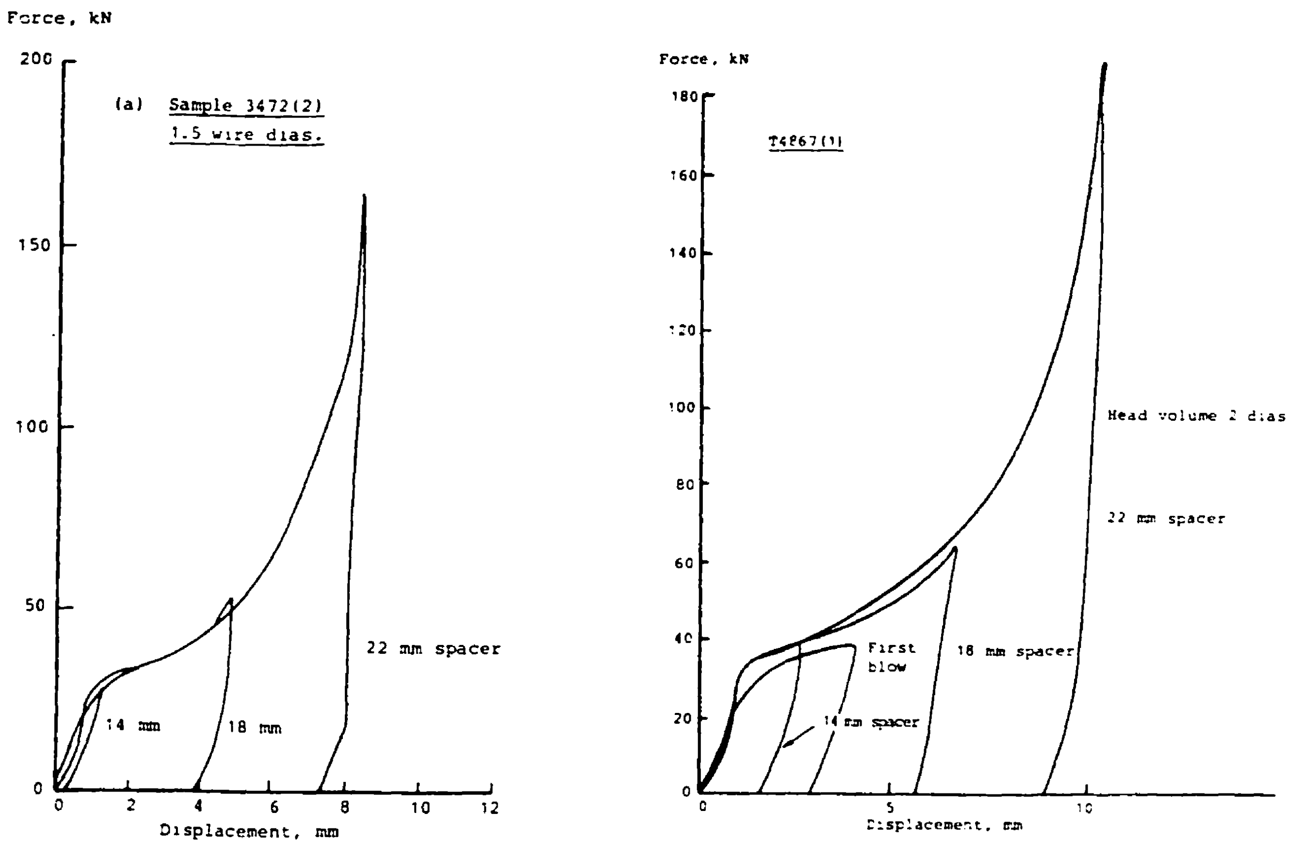

(a) (b)

Figure 2.16[5]

a) Typical force-displacement curve for single blow heading

b) Typical force-displacement curve for double blow heading

2.6.3.1 USE OF FLOW CURVES AND ENERGY CURVES

There are various possible methods of acquiring flow curves. One method used is to perform tensile tests at a speed of 2 mm/min. and measure the cross-section of the sample during testing. The true stress-true strain curve is obtained by using the force measurements and the flow curve can be determined, as illustrated in Figure 2.17. However, as the strains involved in cold heading can be considerably greater than those possible in tensile tests, a more representative flow curve over the complete range of strains encountered in cold heading may also be required. This can be achieved through various methods involving wire drawing.[5]

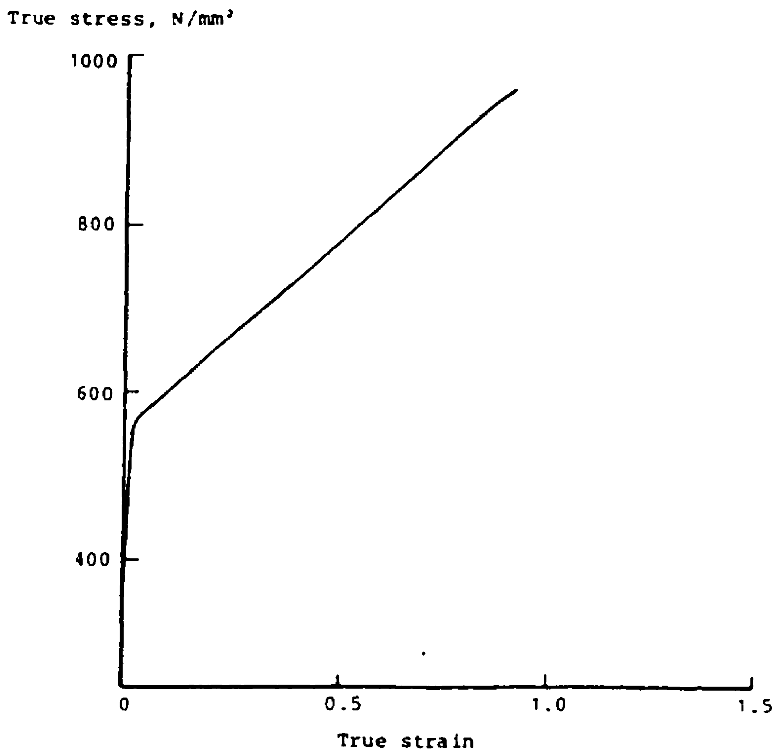

Figure 2.17 - Typical true stress-true strain curve determined by tensile testing[5]

In order to evaluate the cold formability of the specimens tested, a comparison of the energy necessary to produce given strains is required. The work done per unit volume of head is determined graphically through integration of the force-displacement curves and dividing by the head volume. The area under the true stress-true strain curves can also be calculated through a non-linear regression. Both of these work/unit volume values are plotted against true strain to produce energy curves, as shown in Figure 2.18.

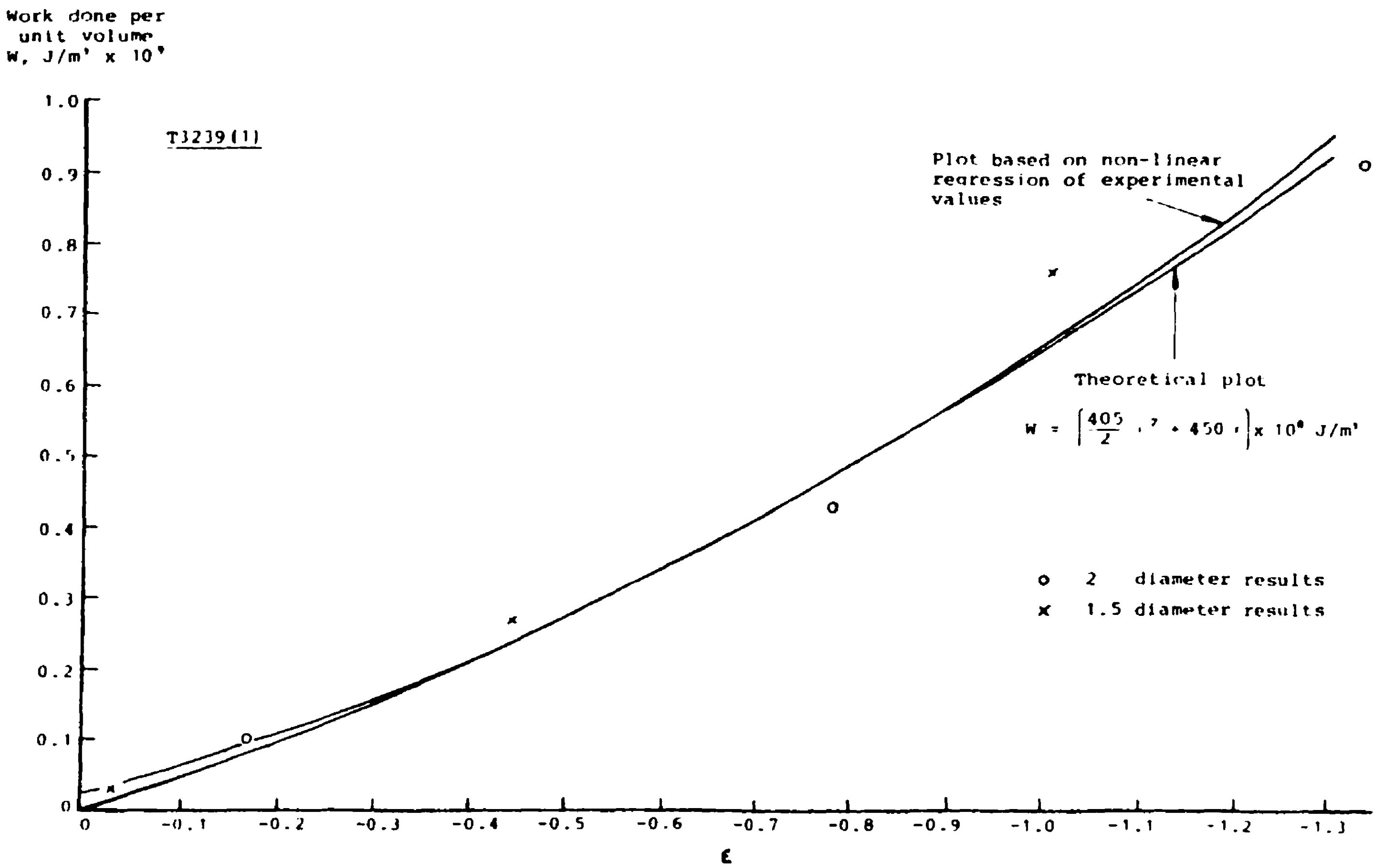

Figure 2.18 - Typical energy curve (work done/unit volume versus true strain)[5]

The energy curve allows a comparison to be made between the work determined from the force-displacement curve obtained from the cold heading tests and those from the true stress-strain curves obtained from tensile tests. While good agreement was found for lower strains and single blows, significant deviations existed at higher strains, particularly for the two-blow heading curves. This might be due to the basic difference between single and double blow upsetting or the extrapolation of the tensile flow curve to these higher strains and strain rates. However, as the strain rate sensitivity of the materials tested is small, this deviation cannot be directly explained by the mechanical strain rate effect.[13] Other factors, undetermined to date, must play a role; one of these could be the effect of deformation heating.

Thus, tests were performed on the instrumented cold heading machine and data were examined as described above in the hope of achieving a direct assessment of the cold formability and ductility of materials under different conditions. In particular, the effects of surface defects, heat treatment, wire drawing and alloy addition on headability were examined. While it was often difficult to produce head bursts with ductile steels, failures could be encouraged by allowing free expansion of the workpiece edge following prestraining. Among the findings was that there is no simple correlation between surface defect depth and failure.[5] Surface defects appeared to act as strain discontinuities rather than stress raisers. Tests also confirmed the benefits of cold reduction by wire drawing with respect to increasing the formability. No direct correlation could be found between failure rate and microstructural state. Alloying additions of manganese and nickel (at average levels of 0.80% and 0.20%, respectively) were found to increase the failure rate in double blow heading, though no change in the required energy was noted. Chromium, up to levels of 0.75%, did not negatively affect formability, possibly due to its ability to stabilize the carbides without changing the flow characteristics of the material.[5]

2.6.4 A NEW UPSET TEST

A new upset test[6] was developed in response to two disadvantages inherent in the conventional version: i) the die shape and the resultant metal flow patterns are substantially different from those experienced in the actual cold heading process; and
ii) the extent of bulging, i.e., the hoop strain, is dependent on the frictional conditions at the die-workpiece interface. The die shape has great influence on the direction and extent of metal flow as well as the fracture location in the specimen. Previous efforts have included the use of various special specimen designs, such as the collared cylinder and the barreled cylinder, to increase the hoop strain to axial strain ratio. This allows for early cracking of the specimen and so increases the sensitivity of the test to surface defects.

However, these specimen shapes modify the billet geometry and so change the process conditions. In addition, they require additional preparation.

The new upset test developed at Ohio State University seeks to represent the actual cold heading process and to minimize the effect of test specific factors, such as changing friction at the die-workpiece interface, through using dies with a relief angle. In addition, it is designed to be easily used by industry, requiring little sample preparation and the use of a simple and reliable testing device.[6]

The experiments were performed on an MTS testing machine with a maximum load capacity of 489 kN. This hydraulic machine was equipped with servomechanical controls for both force and displacement controlled testing. It was operated under displacement control following a sine function in the single cycle mode, simulating the stroke history of a mechanical press. The upset test speed was 12.7 mm/s to maintain similarity to mechanical press speeds.

The die inserts were mounted with shrink rings on the die set. The upper platen of the die set was fixed to the crosshead of the MTS machine and the lower platen to the hydraulic actuator. A cross section of the die assembly is illustrated in Figure 2.19.

The effects of four different die relief angles (0°, 20°, 45° and 90°) on die design were examined by experiments and finite element simulations.[5] All specimens were plain cylinders 23.75 mm in height and 15.88 in diameter. No lubrication was used and compression was not interrupted. As only preliminary experiments were performed to demonstrate the principle and function of the device, solely the load was recorded. The upset ratio was determined by measuring the height of the sample prior to and following deformation.

The specimen ends of samples deformed with die relief angles of 0°, 20° and 45° were supported in die cavities. However, it was found through finite element simulation that changing the die angles did not effect the magnitude of the tensile stresses at the midsection of the specimen, as illustrated in the plot of compressive axial versus tensile hoop strain of Figure 2.20(a). Thus, fracture would occur at the same height reduction regardless of die relief angle as, in these cases, die-billet friction plays an insignificant role in upsetting.

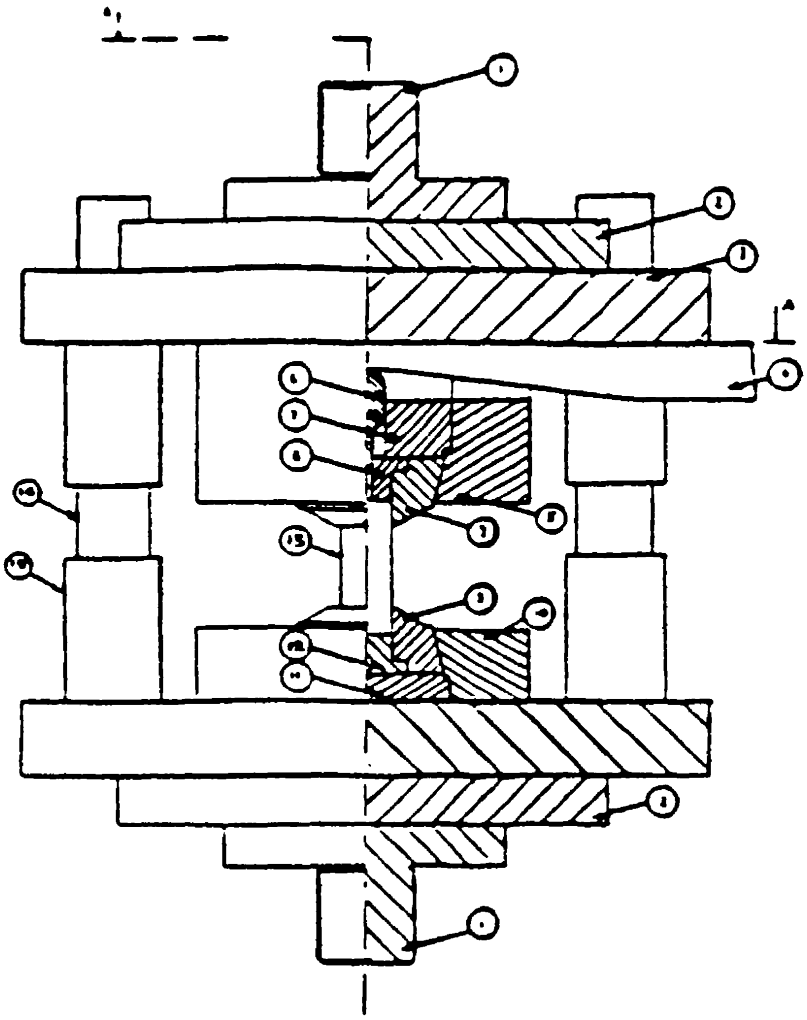

1. Adapter
2. Bolster plate
3. Die set
4. Knock-out lever
5. Shrink ring, top
6. Knock-out pin
7. Pressure plate, top
8. Pressure pad, with hole
9. Conical die inserts
10. Shrink ring, bottom
11. Pressure plate, bottom
12. Pressure pad, bottom
13. Billet
14. Tie rods
15. Guidance columns
16. Cylindrical stops

Figure 2.19 – Cross-section of the die construction showing assembly details[6]

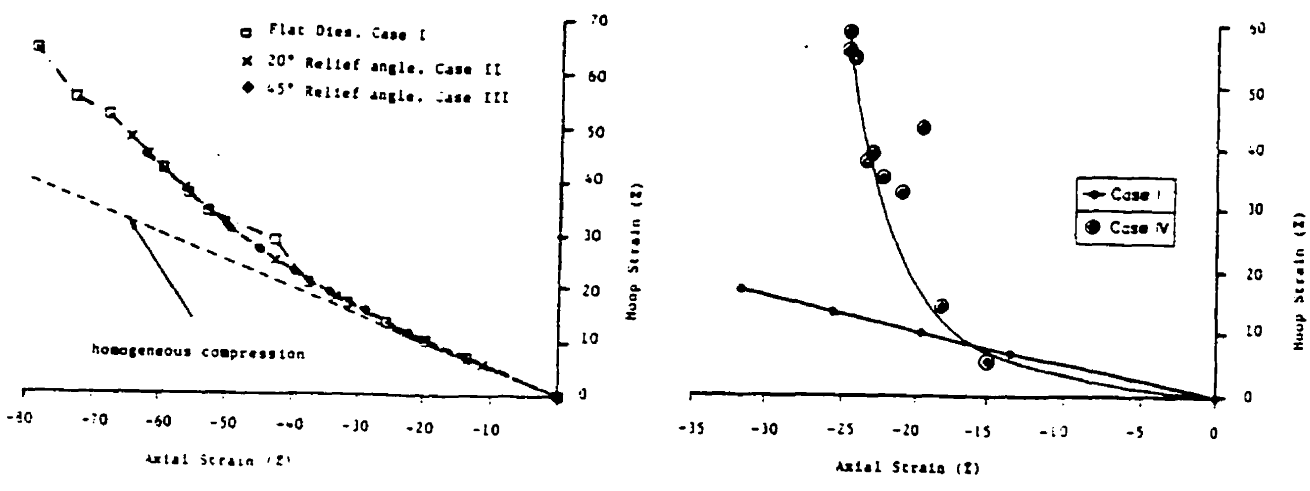

(a) **(b)**

Figure 2.20[6]

a) Plot of axial versus hoop strain for Cases I (α=0°), II (α=20°) and III (α=45°)

b) Plot of axial versus hoop strain for Cases I (α=0°) and IV (α=90°)

Tests were also performed with dies possessing concentric grooves and a relief angle of 90^0; the results obtained are illustrated in Figure 2.21. The grooved dies had the same diameter as the test specimens and a central cone to locate the specimen. Samples possessed matching conical grooves at the centers of the end faces. It was determined that material restriction at the die-specimen interface (sticking friction) resulted in the development of very high tensile hoop strains during upsetting, as seen in the finite element simulation plot of the strains in Figure 2.20(b). Therefore, this test is very sensitive to surface defects, such as seams in hot rolling, and early cracking. As well, in both the experimental and finite element simulation studies, it was noted that a portion of the deforming specimen initially stuck to the side of the die. However, a second sliding mode then started, whereby the material detached itself from the side of the die and the possibility of folding was eliminated.[5] Thus, this test appears to provide an improvement compared to conventional methods.

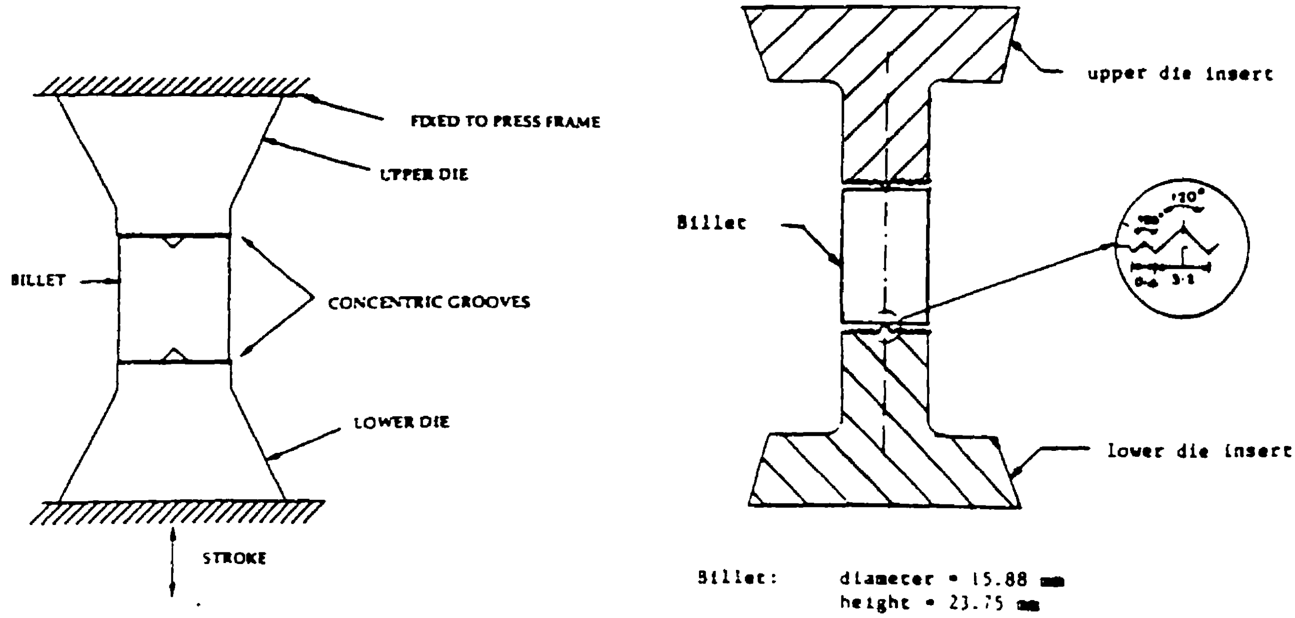

a) Schematic of the test set up for upsetting with concentric grooved dies

b) Cross-sectional view of die-billet configuration for tests with concentric grooved dies

Figure 2.21[6]

2.7 SUMMARY

There are various factors that must be considered when attempting to assess cold headability. These render the use of an accurate and simple test method rather difficult. While the traditional upset test has been used extensively in the past, it is ill-suited to provide a realistic simulation of the cold heading process. A headability impact tester has been developed that is capable of generating data for quantitative headability ratings. Similar results, however, were found to be obtainable through conventional test methods. The split Hopkinson pressure bar tester produces strain rates similar to those experienced in cold heading. Such a piece of equipment, however, requires considerable capital investment and operating expertise. The use of commercial cold heading machines was found to provide a direct assessment of cold formability and ductility. As well, a new version of the upset test has also been developed by Professor Shivpuri and co-workers, which possesses greater sensitivity to surface defects and higher resistance to folding. An adaptation of this revised upset test will be described in the chapters that follow, together with the results obtained from preliminary tests. As well, a drop weight test developed by Nickoletopoulos[20] at McGill University will be discussed and some experimental results obtained using this equipment described.

CHAPTER III

EXPERIMENTAL DETAILS

3.1 UPSET TEST EXPERIMENTS

3.1.1 SAMPLES FOR UPSET TESTING

The materials tested in this study were provided in rod form by Ivaco Rolling Mills. The intention was to obtain known potentially defective and potentially nondefective steel samples. These would then both be tested by the revised upset test in an attempt to validate the ability of the test to differentiate between acceptable and unacceptable headability success rates.

The chemistries of the samples tested are shown in Table 3.1. Part of this steel was thought to be defective due to an incomplete spheroidization heat treatment. Steels A and B, from the Ivaco melt shop, were from a 1541V grade, whereas steel C, from QIT, is a welding grade, 70S-6, that is currently being studied for use as a dual phase steel at Ivaco.

Table 3.1 - Chemical compositions of the samples to be upset in wt%

STEEL	C %	Mn%	V %	N %	P %	S %	Si %	Cu %	Ni %	Cr %	Mo %	Al %
A	0.403	1.420	0.0260	0.0072	0.014	0.035	0.175	0.109	0.062	0.054	0.022	0.004
B	0.381	1.383	0.0260	0.0069	0.018	0.037	0.198	0.176	0.062	0.087	0.013	0.004
C	0.122	1.419	0.007	0.0050	0.017	0.038	0.907	0.031	0.072	0.035	<0.017	0.006

The samples to be upset were machined according to the design of Figure 3.1. The central indentations on the two ends of each specimen were intended to locate the sample centrally on the surface of the lower die.

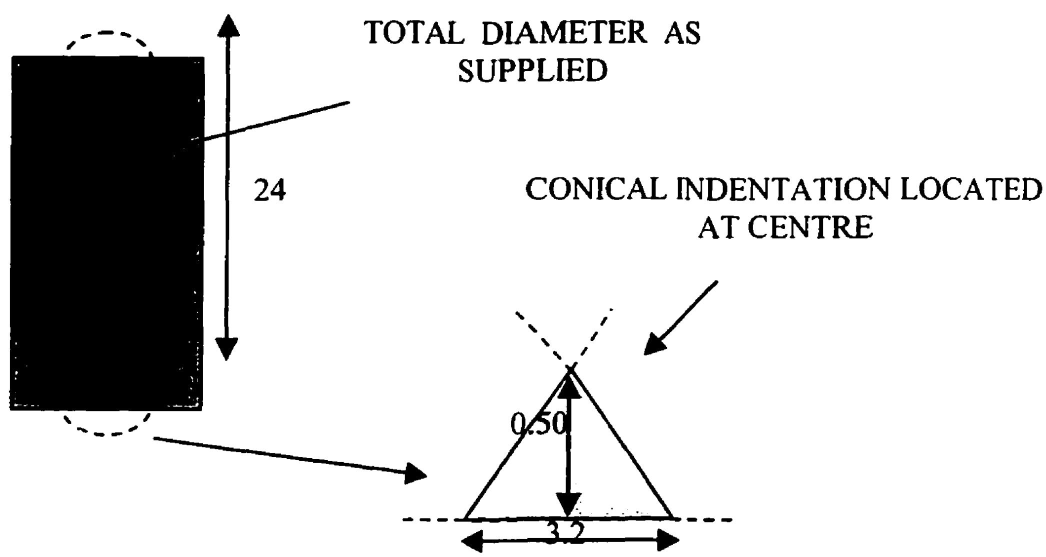

Figure 3.1 – Upset sample design – all measurements in mm (not to scale)

3.1.2 DIE DESIGN

The dies were made of Atlas S7 tool steel. This grade was chosen due to its very high toughness level and stability in hardening. It also possesses suitable wear resistance through alloying with chromium. The chemistry is noted below in Table 3.2.

Table 3.2 – Chemical composition of the die tool steel in wt%

GRADE	C %	Mn %	Si %	Cr %	Mo %
S7	0.50	0.50	0.25	3.25	1.45

The design of the die is shown in Figure 3.2 and that of the die set in Figure 3.3. The die surface ends have conical protrusions at the centres that match those of the samples to be upset tested (0.5 mm maximum height), in addition to concentric grooves of lower heights and angles of inclination machined across the entire surface (0.12 mm maximum height). This is a change from the geometry of the upset test used in research at Ohio State University[6] in that the central cone and concentric grooves are of considerably larger diameter. This was an attempt to decrease the stress concentrations that led to premature fracture of the die in previous experiments[6].

The top and bottom die shanks were inserted into the die set to increase alignment. The shanks were machined with threads at a pitch of 12 per inch. The die set consists of an upper and lower plate and two rear guidance columns.

3.1.3 UPSET TEST EQUIPMENT

The upset tests were performed at the Materials Technology Lab at CANMET with a Materials Testing Systems (MTS) machine. This hydraulic press has a maximum load (force) of 450 kN and is equipped for force and displacement controlled testing. Tests were performed at an approximate speed of 12 mm/s. They were performed without any lubrication to maximize the effect of friction and therefore the ability of the test to be sensitive to any defects present in the samples to be upset.

The upset tests were performed with both the die set mounted on the MTS, as well as with the dies attached directly to the machine. The intention was to upset samples until cracking was apparent to the naked eye. The stress-strain curve would then be analyzed to determine the exact point at which material failure commenced.

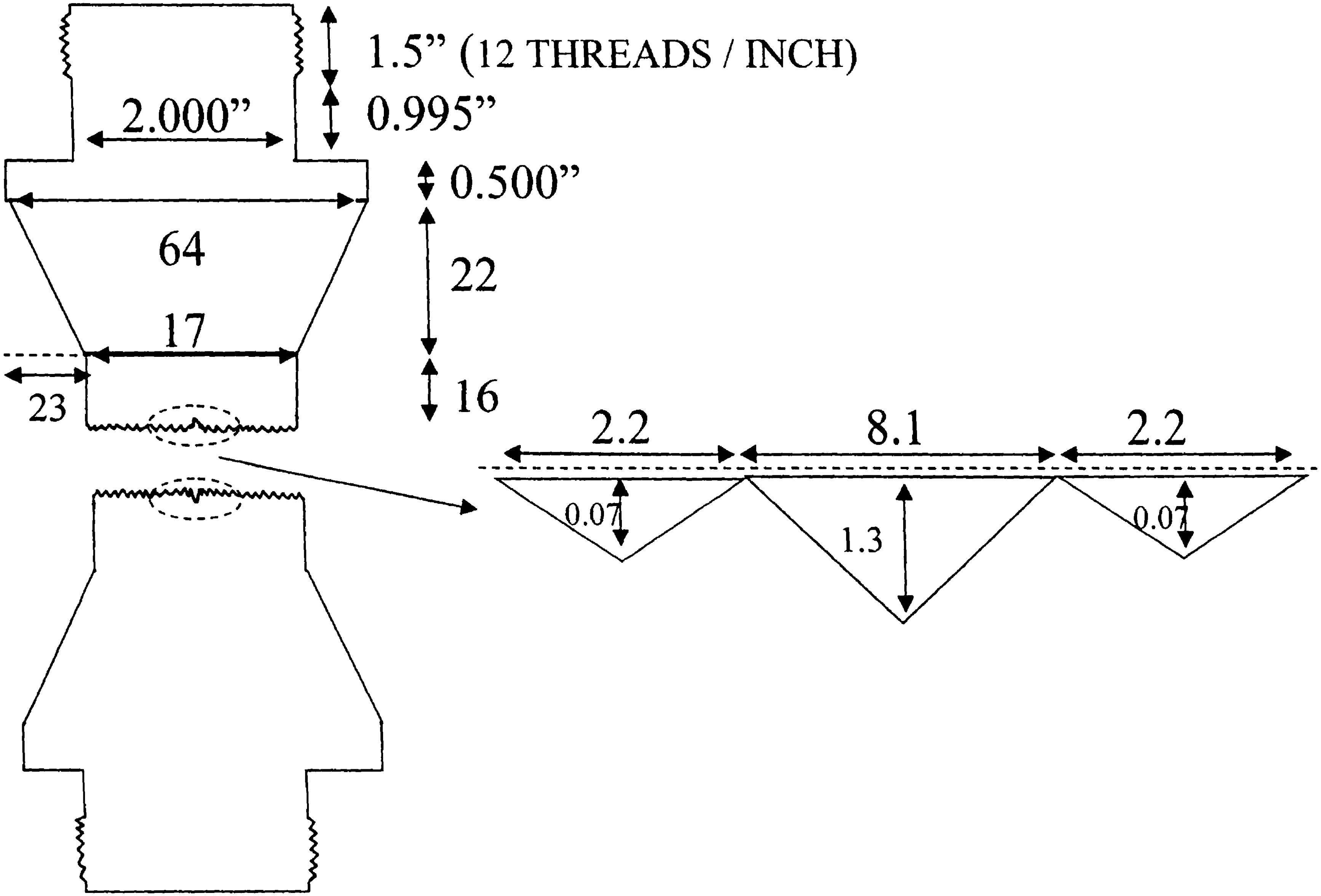

Figure 3.2 – Design of upper and lower dies – all measurements in mm unless otherwise noted (not to scale)

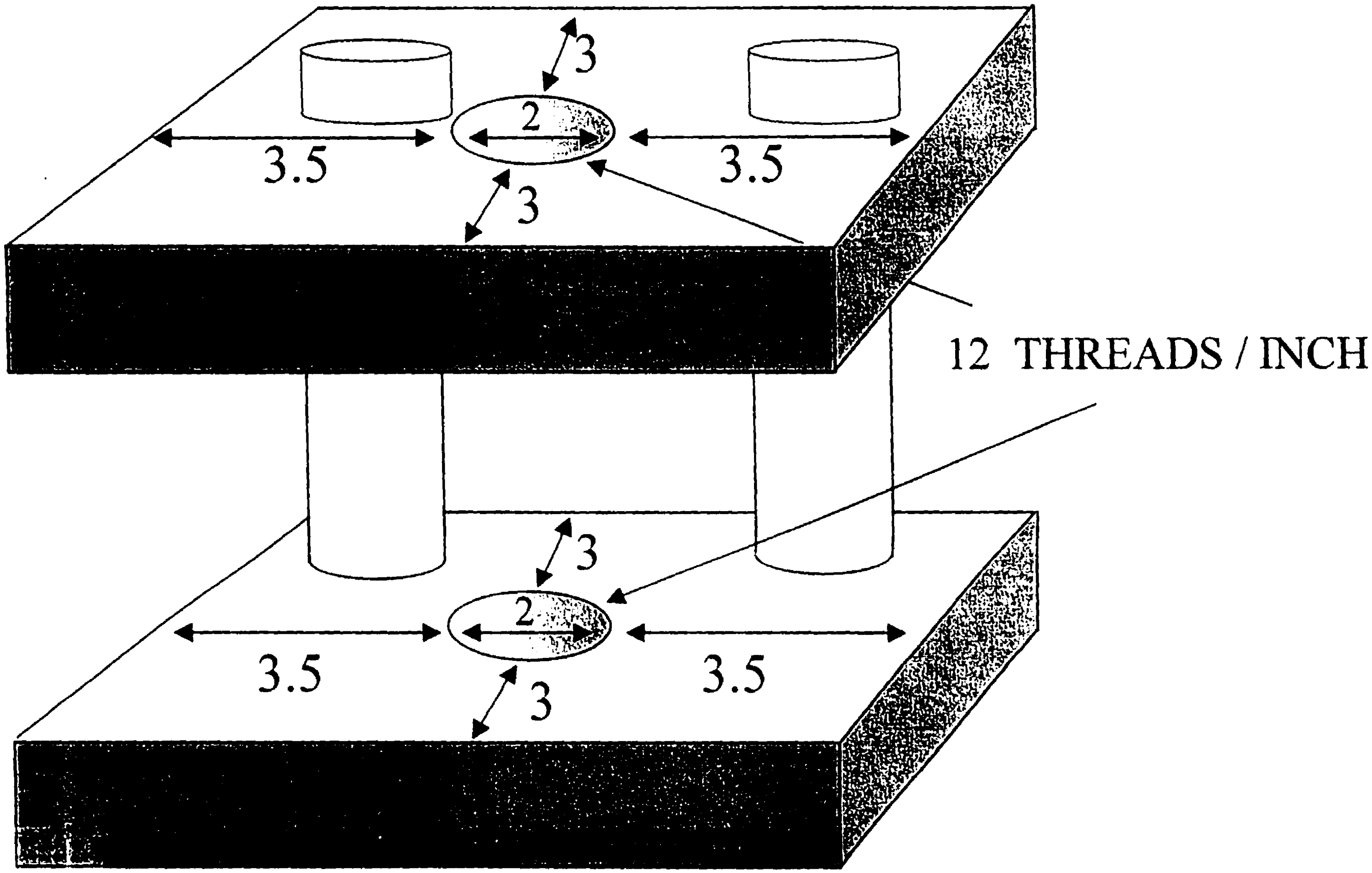

Figure 3.3 - Design of upper and lower die plates – all measurements in inches (not to scale)

3.1.4 SAMPLE ANALYSIS

The upset samples were analyzed metallographically to determine their microstructures. For this purpose, the samples were ground, polished and etched with 4% nital. As well, hardness and tensile test measurements were made on each of the three heats.

3.2 DROP WEIGHT EXPERIMENTS

3.2.1 SAMPLES FOR TESTING

Samples for the drop weight test experiments carried out using the equipment developed by Nickoletopoulos[20] at McGill University were from the same three heats used for the revised upset tests. The chemistries are noted in Table 3.1.

Samples were machined from the drawn diameter of 12.0 mm down to 5.2 mm. Two aspect ratios of 0.6 and 1.0 were used. Ten samples were machined of each aspect ratio for each heat. Five of the ten samples for each heat and aspect ratio had grid lines etched on the surface in an attempt to measure the axial and hoop strains after deformation.

3.2.2 DROP WEIGHT TEST EQUIPMENT

The drop weight test set-up is illustrated in Figure 3.4. A cylindrical support of either 1.27 m or 1.50 m was used to prevent the load from dropping until the test was to be performed. Various weights were used in order to deform the samples to strains that resulted in shear cracking, as well as to strains prior to and after the occurrence of shear cracking. The minimum weight, without any plates added to the load, was 11.77 kg. Each plate added was 1.07 kg. A maximum of seven plates was used during these experiments. Shock absorbers were used to help eliminate the possibility of the load rebounding off the die after the initial impact, causing a second force to be applied to the sample.

3.2.3 DIE DESIGN

The die, illustrated in Figure 3.5 and designed by Nickoletopoulos[20], was constructed of S2 tool steel. A die casing with six cylindrical air vents was used to prevent cracks from developing in the dies. The sample was placed in the centre of the die into a 1.00 mm deep locating inset to ensure secure placement. The locating inset had a 5.25 mm diameter and was tapered to allow the sample to deform within the die

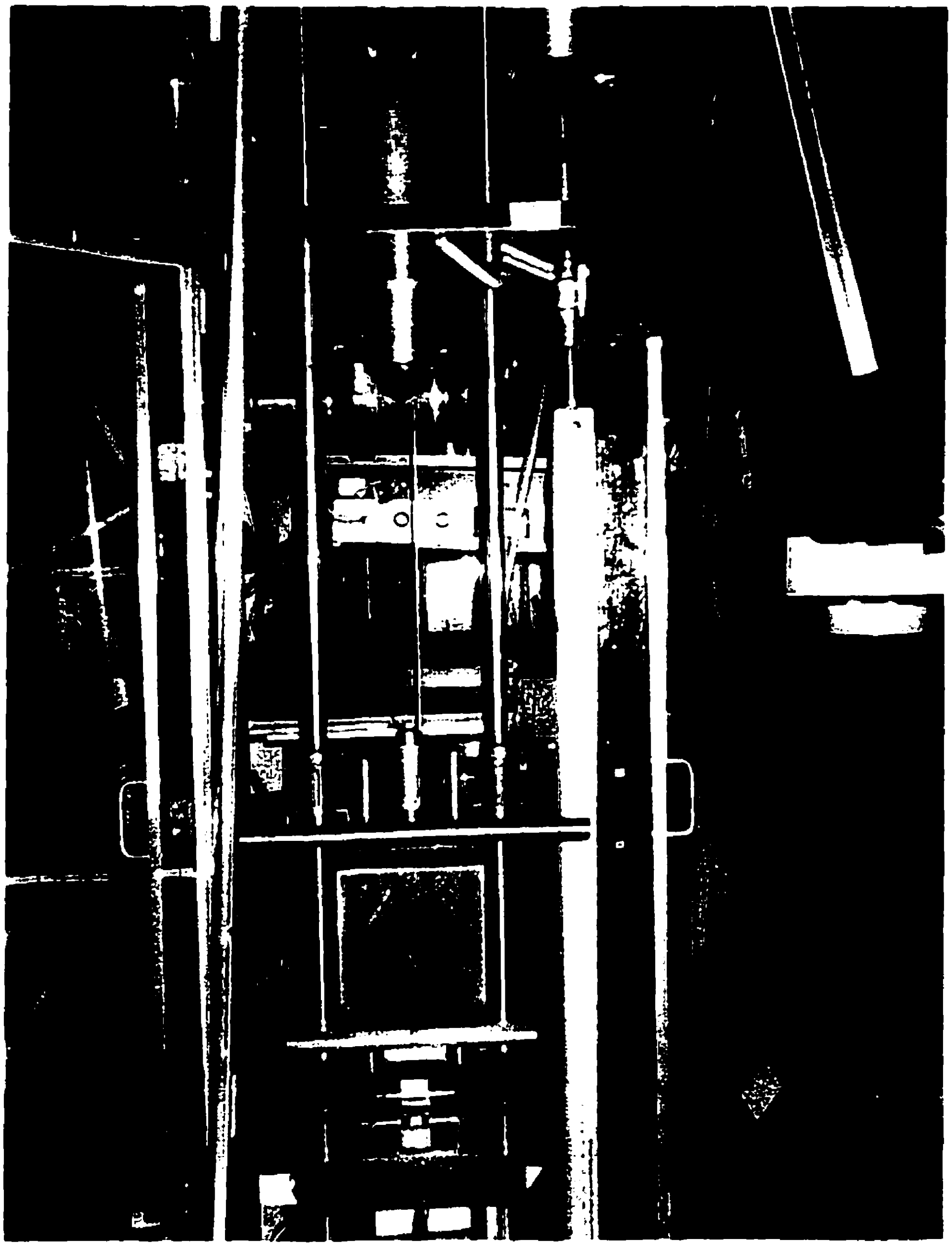

Figure 3.4 - Drop weight test equipment

by approximately 1% in diameter to help prevent die stress build up and cracking of the die. A molybdenum disulfide lubricant was applied to the inset and the flat region of the dies prior to the placement of each sample. This resulted in a friction coefficient of approximately 0.13, as calculated experimentally by Nickoletopoulos[20].

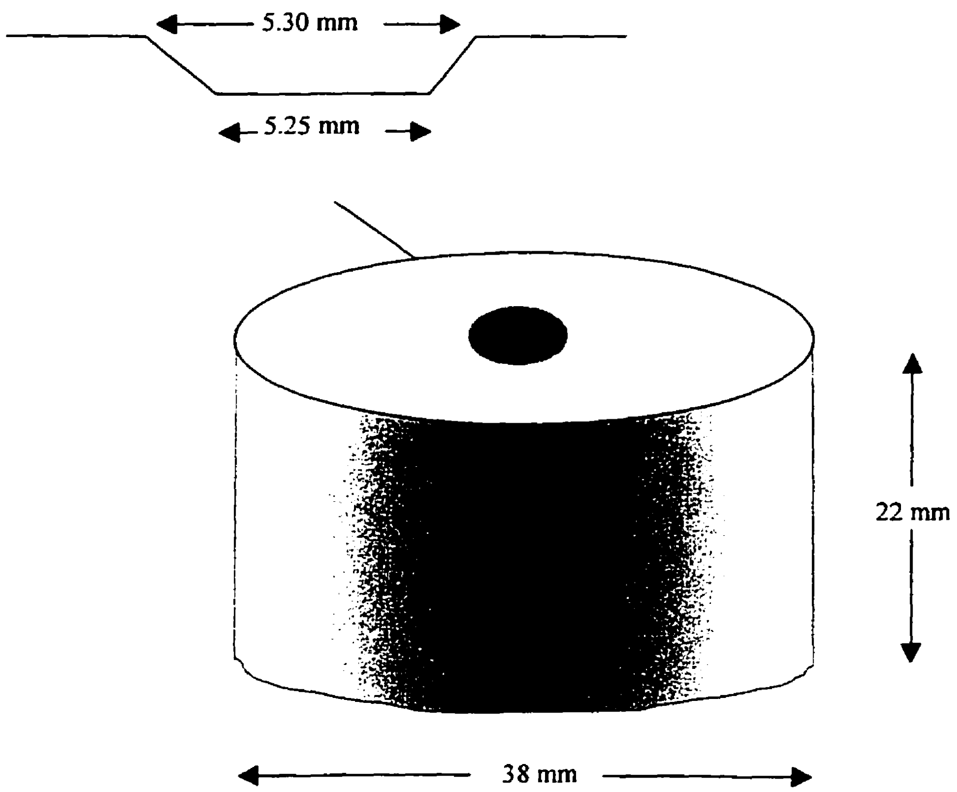

Figure 3.5 - Die design for the drop weight test experiments

3.2.4 SAMPLE ANALYSIS

The deformed and undeformed samples were examined under the SEM to analyze the fracture surface and overall surface quality. Metallographic samples were also prepared by grinding, polishing and applying a 4% nital etch to examine the microstructures of the three heats. Hardness and tensile measurements were also made on each of the three heats, as discussed above.

CHAPTER IV

RESULTS AND DISCUSSION

4.1 REVISED UPSET TESTS

4.1.1 EXPERIMENTAL RESULTS

The initial upset tests were performed with the dies attached to the die set. The first sample was placed in the MTS machine between the upper and lower dies and compression began at a speed of approximately 12 mm/s. This resulted, in addition to compression of the sample, in cracking and then chipping of the ends of the lower die surface. Figure 4.1 illustrates the cumulative damage caused to the bottom die end after several tests were performed, revealing the chipping away of the edge in a distinct region. The compression of the samples, shown in Figures 4.2 a) and b), always commenced on one side, i.e., it is obvious that an uneven load was being applied during deformation. It was on this side that fracture would occur and the sample would split open before the test could be stopped. It was also at this preferred location that chipping of the die occurred. The top and bottom dies were then switched, the die set realigned and further tests performed. However, the same result occurred, with chipping of the die and more severe deformation of the sample commencing in a preferred location on the lower die.

Figure 4.1 – Lower die after several upset tests have been performed – note the chipping on the edge of the testing surface

a) **b)**

Figure 4.2 – Upset samples after deformation and cracking

The dies were then remachined to remove any damage caused by the chipping and further upset tests were performed without the die set. While the intention of the die set was to improve the alignment, it was thought after the first set of experiments that it was probably contributing to the uneven load (because it only had two posts and not four). However, tests using only the upset dies led to results that were similar to those of the original experiments. Despite attempts to achieve alignment, the dies continued to chip in a similar manner and the samples deformed unevenly around the circumference.

4.1.2 SAMPLE ANALYSIS

The microstructures of steels A, B and C are shown in Figures 4.3, 4.4 and 4.5, respectively. Steels A and B are characterized by a microstructure that was not spheroidized. Colonies of pearlite are evident in the ferrite matrix of both microstructures. Steel C, the dual phase material, contains a ferrite matrix with martensite along some of the grain boundaries.

The results of the hardness and tensile measurements made on each of the three heats are summarized in Table 4.1. Steel C possesses the highest level of hardness, followed by steel B and then steel A.

Table 4.1 – Hardness and tensile measurements of the samples to be upset

STEEL	HARDNESS (RB)	TENSILE (MPa)	YIELD (MPa)
A	71.2	554	324
B	77.1	575	331
C	80.3	600	342

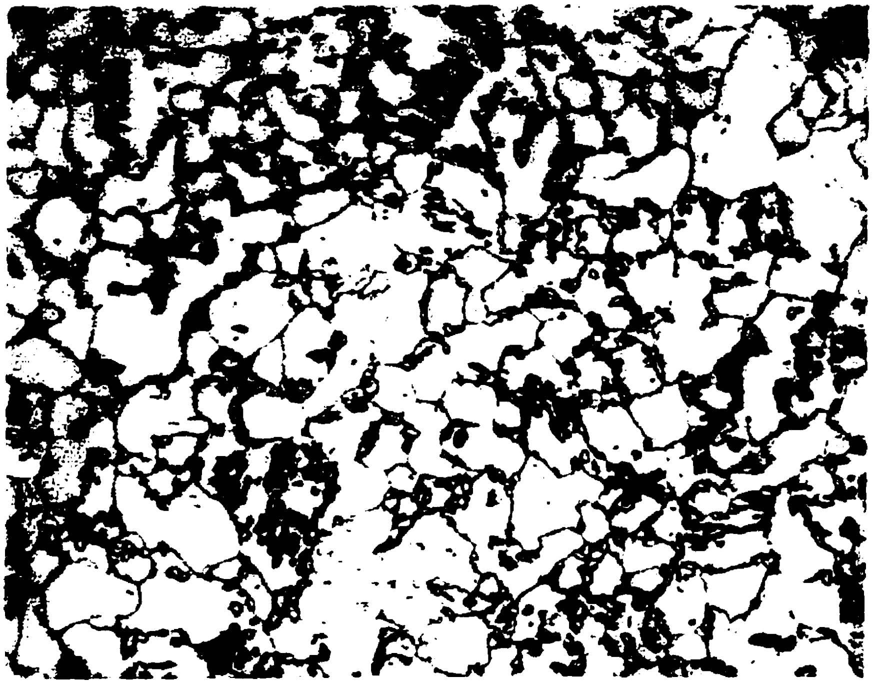

Figure 4.3 – Unspheroidized microstructure of Steel A (4% nital etch – x1000)

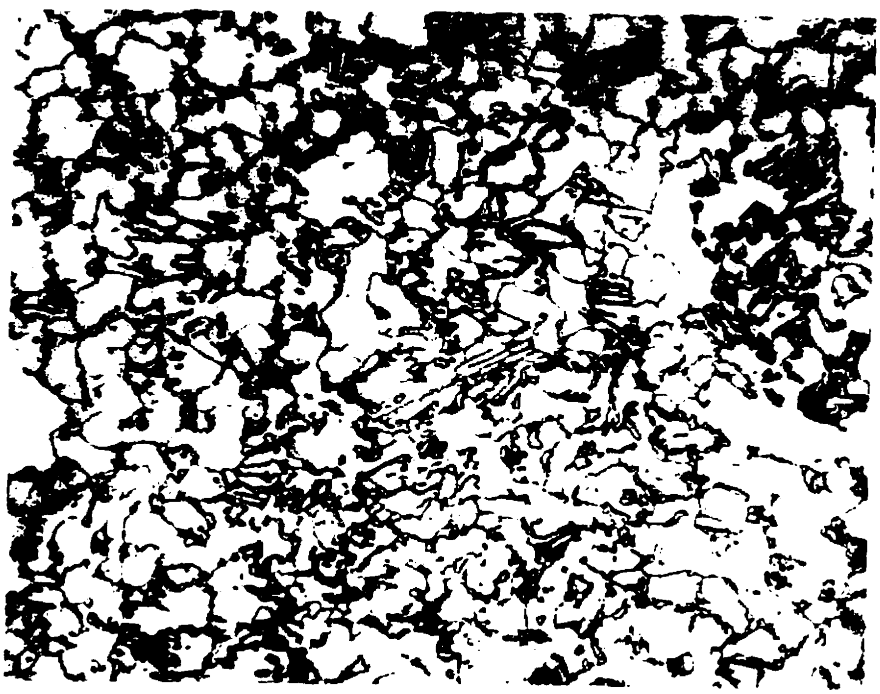

Figure 4.4 – Unspheroidized microstructure of Steel B (4% nital etch – x1000)

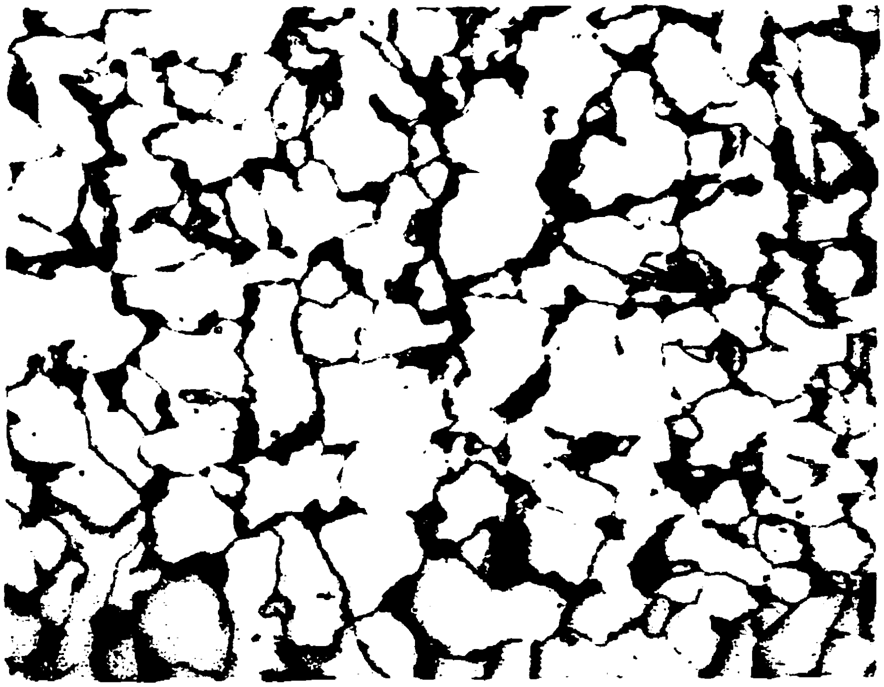

Figure 4.5 – Dual phase ferrite-martensite microstructure of Steel C (4% nital etch – x1000)

4.1.3 POSSIBLE DESIGN FLAWS AND IMPROVEMENTS

The revised upset test obviously was not able to differentiate between various material aptitudes for cold headability. This was due to the uneven rates of deformation applied to the upset samples, resulting in an inaccurate representation of the heading process. A further complication involved the die cracking, which curtailed the number of experiments that could be carried out. An examination of how this could be improved in the future is required.

4.1.3.1 SELECTION OF TOOL STEEL

While the Atlas S7 tool steel was thought to provide sufficient toughness and resistance to cracking for the purposes of this study, perhaps another selection would have prevented premature cracking of the dies. Atlas Ultimo 6 and Monark tool steels possess higher levels of fracture toughness. While their wear resistance is lower, it might be adequate for laboratory studies of the present type (i.e., they have higher C and Mn and lower Cr levels).

4.1.3.2 DIE DESIGN

It is possible that the design of the die, with a central protrusion to match the corresponding conical cavity in the samples to be upset and concentric grooves along the surface ends, could be improved. This would aid in preventing premature cracking. Furthermore, precision machining is required to achieve an identical match between the central cone of the die and the indentation of the sample. Any mismatch in either the machining or in placing of the sample prior to being upset will result in misalignment and an uneven deformation process. There is also the difficulty of aligning the upper and lower dies once they have been attached to the MTS machine. Misalignment between the dies will certainly cause the sample to experience uneven forces.

4.1.3.3 ALTERNATE METHODS

It is possible that the upset test as revised by the present author is not the best method of determining the cold headability. Currently, there is research being conducted at McGill University using FEM modeling to accurately simulate the cold heading process.[20] While a new approach to testing may be difficult to develop initially, once running, it may be better able to reproduce the many factors involved in heading. It may also have the potential to be used for product design.[21,22,23]

While only limited tests were performed with the revised upset test due to the repeated die failures, flow localization in shear was not apparent in the tested samples. Perhaps other means of determining the tendency of a material for shear localization are superior to the revised upset test, such as the drop weight test.

4.2 DROP WEIGHT TEST RESULTS

4.2.1 EXPERIMENTAL RESULTS

Samples of 0.6 and 1.0 aspect ratio from each of the three heats were tested in the drop weight test. Approximate impact velocities of 5.0 m/s and 5.4 m/s were calculated for the tests performed at heights of 1.27 m and 1.50 m, respectively. While the drop weight test normally employs a load cell, it was not functioning at the time these experiments were performed. Therefore, approximate calculations of engineering strain and average force were made based on the sample height reductions. Table 4.2 summarizes these calculations for each sample, as well as the observations of the surface under magnification.

Table 4.2 - Summary of the drop weight test experiments

STEEL SAMPLE	ASPECT RATIO	WEIGHT (kg)	HEIGHT (m)	ENG. STRAIN	F_{AVG} (kN)	SURFACE APPEARANCE
A	0.6	11.78	1.27	0.61	77.2	NO CRACK
		11.78	1.50	0.62	87.0	NO CRACK
		12.84	1.50	0.71	83.1	ONSET OF SHEAR CRACK
		13.90	1.50	0.74	83.4	SHEAR CRACK
	1.0	11.78	1.50	0.63	59.5	NO CRACK
		12.84	1.50	0.69	57.7	NO CRACK
		13.90	1.50	0.72	59.1	NO CRACK
		14.96	1.50	0.75	60.7	ONSET OF SHEAR CRACK
		16.02	1.50	0.78	64.5	ONSET OF SHEAR CRACK
B	0.6	11.78	1.27	0.61	77.6	NO CRACK
		11.78	1.50	0.63	89.3	DUCTILE CRACK
		12.84	1.50	0.69	86.6	SHEAR CRACK
		13.90	1.50	0.73	87.7	NO CRACK
	1.0	11.78	1.50	0.64	85.3	NO CRACK
		12.84	1.50	0.70	86.6	ONSET OF DUCTILE CRACK
		13.90	1.50	0.73	88.5	ONSET OF SHEAR CRACK

Table 4.2 - Summary of the drop weight test experiments (cont.)

STEEL SAMPLE	ASPECT RATIO	WEIGHT (kg)	HEIGHT (m)	ENG. STRAIN	F_{AVG} (kN)	SURFACE APPEARANCE
C	0.6	11.78	1.5	0.64	85.3	NO CRACK
		12.84	1.5	0.70	86.6	GRID MARK
		13.90	1.5	0.73	88.5	NO CRACK
	1.0	11.78	1.5	0.63	58.3	NO CRACK
		12.84	1.5	0.68	59.7	NO CRACK
		13.90	1.5	0.72	59.9	NO CRACK
		14.96	1.5	0.76	60.4	NO CRACK
		16.02	1.5	0.78	64.0	NO CRACK
		17.08	1.5	0.81	66.4	NO CRACK
		19.20	1.5	0.81	73.9	NO CRACK
		20.26	1.5	0.83	75.2	NO CRACK

As previously mentioned, grid marks were applied to the surfaces of half of the drop weight test samples. It was hoped that, by measuring the changes in height and diameter at the mid-height, hoop and axial strains could be calculated. However, as the aspect ratios used were relatively small, it was not possible to make these measurements.

4.2.2 SAMPLE ANALYSIS

The microstructures and hardnesses of steels A, B and C were shown in Figure 4.3 to Figure 4.5 and Table 4.1, respectively. The dual phase steel C possesses the highest hardness and tensile properties, while the unspheroidized steels A and B possess lower hardness values.

Some examples of the appearance of the "side-of-cylinder" surfaces, as seen under the SEM, are shown in Figures 4.6 to 4.8.

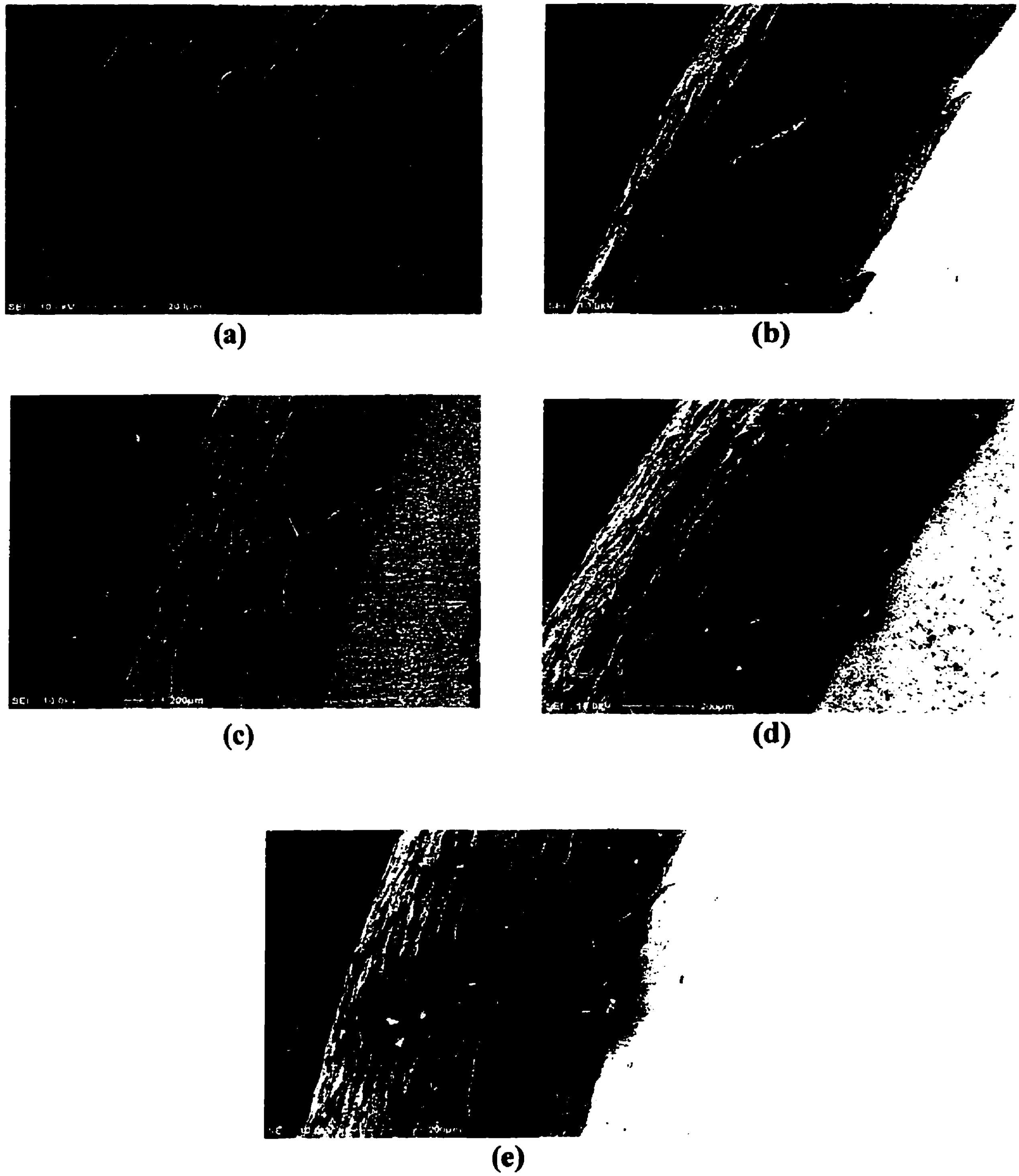

Figure 4.6 – Steel A a) undeformed surface (x90)
b) h/d = 0.6 – onset of shear crack (w=12.84 kg) (x90)
c) h/d = 0.6 – shear crack (w=13.90 kg) (x90)
d) h/d = 1.0 – onset of shear crack (w=14.96 kg) (x90)
e) h/d = 1.0 – onset of shear crack (w=16.02 kg) (x90)

(a)

(b)

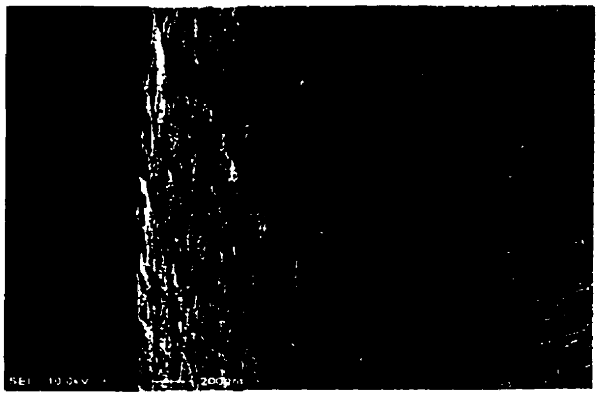

(c)

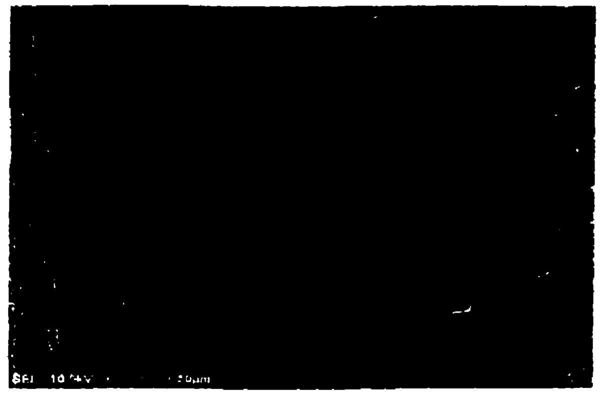

(d)

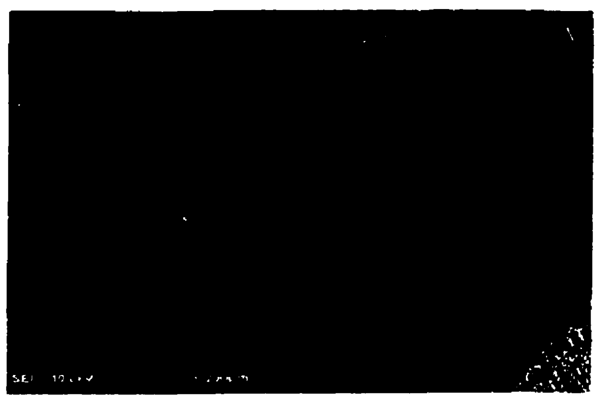

(e)

Figure 4.7 – Steel B a) undeformed surface (x90)
b) h/d = 0.6 – ductile crack (w=11.78 kg) (x90)
c) h/d = 0.6 – shear crack (w=12.84 kg) (x90)
d) h/d = 1.0 – onset of ductile crack (w=12.84 kg) (x250)
e) h/d = 1.0 – onset of shear crack (w=13.90 kg) (x90)

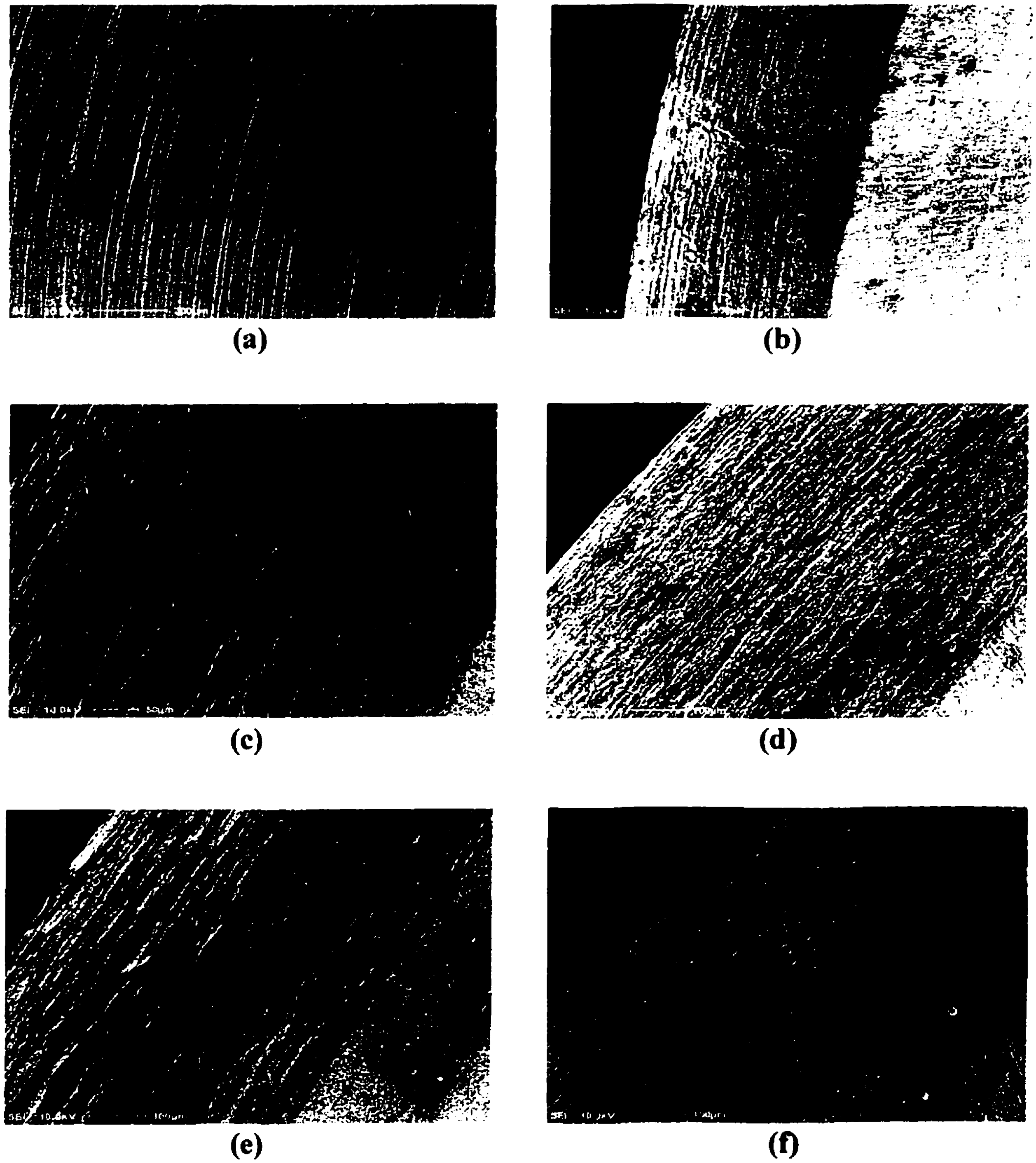

Figure 4.8 – Steel C –a) undeformed surface (x90)
b) h/d = 0.6 – grid mark (w=12.84 kg) (x90)
c) h/d=0.6 – crack not present (w=13.90 kg) (x220)
d) h/d=1.0 – crack not present (w=14.96 kg) (x140)
e) h/d=1.0 – crack not present (w=16.02 kg) (x140)
f) h/d=1.0 – crack not present (w=17.08) (x140)

Figure 4.6 illustrates the surface appearances of steel A after various deformations. The undeformed surface in Figure 4.6 (a) appears to be quite rough. Figures 4.6 (b) and 4.6 (c) illustrate the deformed surfaces of samples with an aspect ratio of 0.6. At an average load of approximately 83.1 kN resulting in an engineering strain of 0.71, the onset of a shear crack is apparent in Figure 4.6 (b). A complete shear crack is obvious in Figure 4.6 (c), at a force of 83.4 kN and an engineering strain of 0.74. Samples with an aspect ratio of 1.0 are shown in Figures 4.6 (d) and 4.6 (e) after engineering strains of 0.75 and 0.78, respectively. The progressive development of a shear crack is clearly revealed.

The various surfaces of steel B samples are shown in Figure 4.7. The undeformed sample, shown in Figure 4.7 (a), appears smoother than that of the undeformed steel A sample. The finish produced by the machining, however, still reveals fine lines. Samples with an aspect ratio of 0.6 exhibited a ductile crack at an average load of 89.3 kN and an engineering strain of 0.63, shown in Figure 4.7 (b). Figure 4.7 (c) illustrates a shear crack at a load of 86.6 kN and an engineering strain of 0.69. Samples with an aspect ratio of 1.0, shown in Figures 4.7 d) and 4.7 (e), do not reveal complete shear crack formation. At a load of 57.9 kN and strain of 0.69, Figure 4.7 (d) reveals the commencement of a fine ductile (longitudinal) crack. The onset of a shear crack is shown in Figure 4.7 (e), at a load of 58.2 kN and a strain of 0.75.

Figure 4.8 reveals the surface appearances of steel C. The undeformed sample, shown in Figure 4.8 (a), exhibits the fine lines resulting from machining, similar to those of steel B. The surfaces of samples with aspect ratios of 0.6 and 1.0 at various loads and strains, illustrated in Figures 4.8 (b) through 4.8 (f), do not reveal any ductile or shear cracks. One of the fine grid lines that was etched onto half of the samples is shown in Figure 4.8 (b) on a sample with an aspect ratio of 0.6. Under lower magnification, this was initially thought to be a crack and only one further test at a higher load was conducted. Tests on samples with an aspect ratio of 1.0 were conducted with masses of up to 20.26 kg, resulting in an average load of 75.2 kN and an engineering strain of 0.83. Cracks were not observed at any of the load increments on these samples.

Based on the drop weight tests described above, the applied strains resulted in shear cracking in steels A and B. Steel C, however, did not reach the point of fracture. This is possibly explained by the difference in microstructure. Steels A and B were unspheroidized, and, consequently, their formability was limited. Steel B also possessed higher levels of Cr and Cu than steel A, increasing the hardness of steel B and therefore decreasing its formability relative to steel A. Steel C displayed a dual phase microstructure. Although steel C was the hardest of the three steels, it was also the most formable. This can possibly be explained by the strong (martensite) yet ductile (ferrite) nature of dual phase steels. In addition, steel C possessed a significantly lower nitrogen content relative to steels A and B. This would have helped to minimize instabilities resulting in sudden shear softening. The presence of solute nitrogen in steels A and B, for example, may produce dynamic strain aging in these materials and cause them to display negative rate sensitivities. Such negative rate sensitivities are well known to promote flow localization. Therefore, the strains developed during these experiments, while sufficient to cause cracking in the unspheroidized steels, were not capable of developing shear cracks in the more formable dual phase samples. Consequently, the drop weight test appears to be capable of distinguishing between headable and less headable steels.

4.2.3 EFFECT OF ASPECT RATIO

The effect of aspect ratio, illustrated in Figure 2.5, is evident throughout these experiments. The lower the aspect ratio, the less compressive strain is required to reach the formability limit of the sample. This is because there is less interior material supporting the surface material and so sample bulging (circumferential strain) develops at a lower nominal (height) strain. Steel A samples with an aspect ratio of 0.6 displayed shear cracking. Those with an aspect ratio of 1.0, even at higher engineering strains, exhibited only the *onset* of shear cracking. While steel B appeared slightly less formable overall than steel A, the same pattern was observed. In addition to actual cracking, there is a difference in the general surface quality between the two aspect ratios in steel B. Those with the lower aspect ratio display a general rupturing of the surface, illustrated in Figure 4.7 (c). However, samples with the higher aspect ratio, shown in Figures 4.7 (d) and (e), do not have nearly the same level of roughness imparted to the surface, as higher strains are required to reach their formability limits.

4.2.4 EFFECT OF SAMPLE MACHINING

As noted previously, all samples were machined down from the drawn diameter of 12 mm to 5.2 mm in order to accommodate the die design. By removing the exterior 6.8 mm of the steel, surface defects were also eliminated. This has the advantage of allowing the true formability of the steel to be determined. However, this also results in losing the capability of testing the actual headability of a specific heat, which is partly determined by surface quality. By removing the surface layer, particularly any rolling defects that are present, a higher formability rating will be determined than would actually occur in a cold heading operation.[20]

While machining does remove the surface defects resulting from the rod manufacturing process, it is difficult to produce a surface finish through machining that is truly smooth. As seen in the SEM photos of the undeformed samples, fine lines are apparent which might act as stress risers. A possible approach to producing a smoother surface would be to grind and polish the samples after machining. This is being investigated by Nickoletopoulos[20].

CHAPTER V

CONCLUSIONS

It was the intent of this research to review the current methods employed for determining cold headability. Experiments were then performed on "formable" and "less formable" steel samples on a revised upset tester and on a drop weight tester to determine if they were capable of determining the relative headability. The following conclusions can be drawn from this work.

1. REVISED UPSET TEST EXPERIMENTS

- The revised upset test was unable to determine the headability of the steel samples due to die fracture.
- While flow localization occurred in the samples, shear cracks indicating the point at which the formability of the steel had been reached were not observed.
- The main cause for die fracture was misalignment of the dies in the MTS machine.

- Tool steel selection for the dies possibly played a role in die fracture as well. Grade S7 did not appear to possess sufficient toughness to withstand the loads applied to the dies.

2. DROP WEIGHT TEST EXPERIMENTS

- The drop weight test appears to be able to differentiate between the formable and less formable steel samples.
- Those samples which were less headable displayed shear cracks, while those that were more headable did not at the loads applied and the strains employed in this work.
- The effect of aspect ratio was demonstrated, with those samples with aspect ratios of 0.6 reaching their formability limits earlier than those with the higher aspect ratio of 1.0.
- The dual phase samples displayed the highest hardness value, as well as the highest level of formability. This can possibly be explained by the nature of dual phase steel, as well as its lower nitrogen content relative to the other samples.
- It would be useful to modify the drop weight test equipment to permit the testing of *full size* samples over most of the range of diameters produced industrially.

CHAPTER VI

SUGGESTED FUTURE WORK

While the revised upset test was not successful with the design described in this work, it is possible that through several refinements it could be used to rate headability. A change in die tool steel to S2 might improve its resistance to cracking. In addition, the diameter could be increased to be slightly greater than that of the samples and a centre locating inset machined, similar to the drop weight test die design. A die casing could be added around the die, which proved helpful in preventing die cracking in the work conducted by Nickoletopoulos.[20]

The drop weight test appeared successful in rating headability. However, more extensive experiments should be conducted on various grades and potential levels of formability to confirm this. Further refined weight increments can also be evaluated to determine the exact point at which the formability limit is reached.

REFERENCES

1. Sowerby, R., O'Reilly, I., Chandrasekaran, N. & Dung, N. L.
Materials Testing for Cold Forging
Journal of Engineering Materials and Technology, vol. 106, pp.101-106, Jan., 1984.

2. Dannenmann, D. E. & Blaich, D. M.
Method for Determining Cold Heading Suitability
Wire, vol. 29, no. 2, pp. 84-88, 1980.

3. Muzak, N., Naidu, K. & Osborne, C.
New Methods for Assessing Cold Heading Quality
Wire Journal International, pp. 66-72, Oct. 1996.

4. Yoo, Sun-Joon, Lee, Duk-Lak & Jung, Dong-Taek
Prediction of Cold Heading Quality With High Strain Rate Compression Tester
Proceedings of the Annual Convention of the Wire Association Int., Wire Association Int. Inc., Guilford, CT., USA, pp. 235-240, 1996.

5. Turner, A.F., Betteridge, C. S. & Avery, J.
Development of Steels for the Fastener and Cold Forging Markets by Testing Under Fastener Production Conditions
British Steel Report, Commission of the European Communities, 1984.

6. Shivpuri, R., Kropp, E., Lilly, B. & Tietmann, A.
Formability Testing of Steels for Cold Forming
Near Net Shape Manufacturing Conference, ASM International, pp. 169-177, 1988.

7. *Cold Heading*
ASM Metals Handbook, 9^{th} ed., vol. 14.

8. Maheshwari, M. D., Dutta, B. & Mukherjee, T.
Quality Requirements for Cold Heading Grades of Steel
Tool & Alloy Steels, pp. 247-251, July, 1978.

9. Crawford, J. D., Dunn, R. G. & Humphrey, J. H.
The Influence of Alloying Elements on the Cold Deformation of Steel
Source Book on Cold Forming, American Society for Metals, pp. 140-148, November, 1964.

10. Ohmori, A., Matsuzaki, A. & Amano, K.
Effect of Cu, Sn and Sb on Cold Forgeability of a 0.5% Carbon Steel
ISIJ International, vol. 37, no. 3, pp. 302-304, 1997.

11. Dhers, J., Thivard, B. & Genta, A.
Improvement of Steel Wire for Cold Heading
Wire Journal International (USA), vol. 25, no. 10, pp. 73-76, Oct. 1992.

12. Kudo, H., Sato, K. & Aoi, K.
On Cold Forgeability Test
Annals of the C.I.R.P., vol. 16, pp. 309-318, 1968.

13. Jenner, A. & Dodd, B.
Cold Upsetting and Free Surface Ductility
Journal of Mechanical Working Technology, vol. 5, pp. 31-43, 1981.

14. Lee, P. W. & Kuhn, H. A..
Cold Upset Testing
Workability Testing Techniques, ASM, pp. 37-50, 1984.

15. Wodall, S. M. & Schey, J. A.
Determination of Ductility for Bulk Deformation
Formability Topics - Metallic Materials, ASTM STP 647, pp. 191-205, 1978.

16. Shah, J. J. & Kuhn, H. A.
An Empirical Formula for Workability Limits in Cold Upsetting and Bolt Heading
Journal of Applied Metalworking, vol. 4, no. 3, pp. 255-261, 1986.

17. Darvas, Z.
The Forming Limit and the Fracture Mode in Cold Upsetting
Materials Science & Engineering, vol. 70, pp. 101-110, 1985.

18. Lee, P. W. & Kuhn, H. A.
Fracture in Cold Upset Forging - A Criterion and Model
Metallurgical Transactions, vol. 4, pp. 969-973, April 1973.

19. Follansbee, P. S
High Strain Rate Compression Testing
ASM Metals Handbook - "Mechanical Testing" 9th ed., vol. 8.

20. Nickoletopoulos, N.
Experimental Determination and Numerical Modelization of Strain and Fracture in Upsetting for Cold Heading Operations.
Ph.D. Thesis, McGill University, 2000.

21. Predeleanu, M., Cordebois, J. P. & Belkhiri, L.
Failure Analysis of Cold Upsetting by Computational and Experimental Simulation
Conf. Proc. on Numerical Methods in Industrial Forming Processes, Gothenberg, Sweden, Aug. 25-29, 1986, A. A. Balkema, Rotterdam, Netherlands, pp. 277-282, 1986.

22. Sekhon, G. S., Arora, K. S. & Shishodia, K. S.
Application of Finite-Difference and Finite Element Methods to the Axisymmetric Cold Heading Process
Conf. Pro. on Computational Plasticity: Models, Software and Applications-Part II Barcelona, Spain, Apr. 6-10, 1987, Pineridge Press, Swansea, U.K., pp. 1061-1071, 1987.

23. Vertin, K. D. & Majlessi, S. A.
Finite Element Analysis of the Axisymmetric Upsetting Process Using the Deformation Theory of Plasiticity
Transactions of the ASME, vol. 115, pp. 450-458, Nov. 1993.

24. Agarwal, P. & Hone, M.
On-Line Eddy Current System for Evaluation of Cold Heading Quality Wire Rod
Fastener Age, vol. 1, no. 2, pp. 35-41, Nov.-Dec. 1987.

25. Baralis, G., Farinet, M. & Guglielmi, F.
In Line Heat Treatment of Austenitic and Ferritic Stainless Steel Wire
Ironmaking & Steelmaking, vol. 15, pp. 195-201, 1988.

26. Bhatnager, S. S.
Cold Heading of Steels
Tool Alloy Steels, vol. 12, no. 4, pp. 121-125, April 1978.

27. Boratto, F., Macedo dos Santos, R. & Castilho de Avellar, R.
Dual-Phase Steel for 8.8 Strength Class Fasteners
Wire Journal International, pp. 70-73, Sept. 1993.

28. Cockcroft, M. G. & Latham, D. J.
A Simple Criterion of Fracture for Ductile Metals
National Engineering Laboratory Report No. 240, July 1966.

29. Couque, H. & Walker, J. D.
On the Use of the Compression Split Hopkinson Pressure Bar to High Strain Rate
Journal de Physique IV, vol. 4, col. 8-9, pp. 23-28, Sept. 1994.

30. DeSisto, T S.
<u>*Instrumented Impact Testing.*</u>
76^{th} Annual Meeting ASTM, Philadelphia, PA., USA, June 24-29, 1973.

31. Dieter, G. E.
Overview of Workability
<u>Workability Testing Techniques</u>, ASM, pp. 1-20, 1984.

32. Dolzhenkov, I.E., Verboloz, V. D., Boiko, O.V., Lukash, T. U. & Klimenko, A.P.
Improving Quality of Coiled Rod for Cold Heading
Stal', no. 5, pp. 65-67, May 1988.

33. El-Magd, E.
Mechanical Properties at High Strain Rates
Journal de Physique, vol. 4, col. 8, pp. 149-170, Sept. 1994.

34. *Experience and Technology in Continuous Casting of High Quality Steel*
World Steel Metalwork, Export Man., pp. 149-152, 154-155, 1980-1981.

35. Faessel, A.
New Product Control Technologies - The Case of Long Engineering Steel Products
Iron & Steel Making, pp. 37-43, Jan. 1996.

36. Fang, Jun & Shao, Xianghe.
Analysis of Surface Crack In Cold Heading High Strength Bolt
Heat Treatment of Metals, no. 10, pp. 25-28, Oct. 25, 1994.

37. Field, J. E., Walley, S. M., Bourne, N. K. & Huntley, J. M.
Experimental Methods at High Rates of Strain
Journal de Physique IV, vol. 4, col. 8-9, pp. 3-22, Sept. 1994.

38. Follansbee, P.S. & Frantz, C.
Wave Propagation in the Split Hopkinson Pressure Bar
Journal of Engineering Materials and Technology, vol. 105, pp. 61-66, Jan. 1993.

39. Guthrie, R. M.
An Analysis of the Effect on Cold Headers and Cold Headed Products of Using Annealed Versus Nonannealed Boron-Treated Steel
Wire Association International Inc., 51^{st} Annual Convention, Atlanta, GA, pp. 195-207, 1981.

40. Harding, J.
Mechanical Properties at High Rates of Strain-1979.
Proceedings of 2nd Conference, Oxford, March 28-30, 1979.

41. Hartley, K. A., Duffy, J. & Hawley, R. H.
Measurement of the Temperature Profile During Shear Band Formation in Steels Deforming at High Strain Rates
Army Research Office Report No. DAAG 29-85-K-0003/2, Materials Research Laboratory, Brown University, March 1986.

42. Hone, M., Bernique, D. M. & Krzakowski, A. C.
Real-Time Measurement and Acquisition of Wire Rod Size and Profile at Ivaco Rolling Mills
Proceedings of the Annual Convention of the Wire Association Int., Wire Association Int. Inc., Guilford, CT., USA, pp. 38-43.

43. *Impact Testing of Metals.*
72nd Annual Meeting ASTM, Atlantic City, N.J., USA, June 1969.

44. Kal'ner, V. D., Pustovalov, V. I., Beilin, B. I., Shinkarev, I.F. & Vinokurov,G.V.
Development and Testing of Cold Headed Steel 172G
Steel USSR, vol. 9, no. 9, pp. 480-482, Sept. 1979.

45. Kardos, G.
A Study of Plastic Flow in Steel at High Rates of Strain.
Mechanical Eng., McGill University, 1965.

46. Kardos, G.
Response of Metals to High Strain Rates.
Mechanical Eng. Research Lab., McGill University, May, 1964.

47. Kawakami, H., Koarai, J., Kato, T. & Ashida, S.
Cold Heading Wire for High Duty Bolts
Wire Industry, vol. 54.

48. Kessler, S. L., Adams, G. C., Driscoll, S. B. & Ireland, D. R.
Instrumented Impact Testing
Symposium by ASTM, Houston, TX, USA, March 11-12, 1985, ASTM, 1986.

49. Lehnert, W.
Production and Use of High Strength Cold Heading Steels
Wire, vol. 45, no. 5, pp. 275-280, 1995.

50. Mani, R.
Investigation of Stem Crack Formation and Its Reduction in Cold Heading Steering Yoke
Master of Science Thesis, Ohio State University, 1997.

51. Matsunga, T. & Shiwaku, K.
Manufacturing of Cold Heading Quality Wire Rods and Wires
SEAISI Q., vol. 9, no. 1, pp. 45-55, Jan. 1980.

52. McClintock, F. A.
A Criterion for Ductile Fracture by the Growth of Holes
Journal of Applied Mechanics, pp. 363-371, June 1968.

53. Michel, B. & Boyer, J. C.
Elasto-visco-plastic Finite Element Analysis of a Cold Upsetting Test and Stress State Validation by Residual Stress Measurements
Journal of Materials Processing Technology, vol. 54, no. 1, pp. 120-128, 1995.

54. Mullins, W. M., Irwin, R. D., Malas III, J. C. & Venugopal, S. V.
Examination on the Use of Acoustic Emission for Monitoring Metal Forging Process: A Study Using Simulation Technique
Scripta Materialia, vol. 36, no. 9, pp. 967-974, 1997.

55. Nguyen, C. H.
On the Asymmetrical Material Flow in Metal Specimens Under Dynamic Compression with Hopkinson Bars
Journal de Physique IV, vol. 4, col. 8-9, pp. 95-100, Sept. 1994.

56. Nozaki, T., Kawahara, M., Mori, T. & Yao, Y.
Horizontal Continuous Casting of Stainless at Kobe Steel
Iron and Steel Engineer., vol. 62, no. 10, pp. 50-56, Oct. 1985.

57. Oh, S. I.
Finite Element Analysis of Metal Forming Processes With Arbitrarily Shaped Dies
International Journal of Mechanical Science, vol. 24, no. 8, pp. 479-493, 1982.

58. Okamoto, T., Fukuda, T. & Hagita, H.
Material Fracture in Cold Forging - Systematic Classification of Working Methods and Types of Cracking in Cold Forging
Source Book on Cold Forming, ASM, pp. 216-226, 1975.

59. Osman, K.A. & Jones, R.
The Use of Template Matching for In-Process Quality Assessment of Cold Headed Components
CAD/CAM and FEM in Metal Working, Pergamom Press, pp. 103-120, 1988.

60. Parry, D. J., Dixon, P. R., Hodson, S. & Al-Maliky, N.
Stress Equilibrium Effects Within Hopkinson Bar Specimens
Journal de Physique IV, vol. 4, col. 8-9, pp. 107-112, Sept. 1994.

61. Pauskar, P. & Shivpuri, R.
Development of Guidelines to Prevent Internal Cracking During Induction Heating of Cold Forged Parts
North American Manufacturing Research Conference, Houghton, MI, pp. 47-53, May 24-26 1995.

62. Pickering, F. B.
Physical Metallurgy and the Design of Steels.
Applied Science Publishers Ltd., Essex, England, 1978.

63. Rohde, R. W., Butcher, B. M., Holland, J. R. & Karnes, C. H., ed.
Metallurgical Effects at High Strain Rates.
The Metallurgical Society of AIME, Plenum Press, 1973.

64. Semiatin, S. L. & Jonas, J. J.
Formability and Workability of Metals - Plastic Instability & Flow Localization
American Society for Metals, Metals Park, OH, 1984.

65. Schrems, K. K., Laird II, G. & Duttlinger, N. W.
Development of an Instrumented Impact Test For Wire
Wire Journal International, pp. 68-75, Jan. 1995.

66. Semiatin, S. L.
Workability in Forging
Workability Testing Techniques, ASM, pp. 197-247, 1984.

67. Shah, D. C.
Use of Metallic Materials to Model the Flow Fracture of Steel in Cold Upsetting
Conference on Mechanical Working and Steel Processing XII, Dolton, Illinois, USA, Jan. 23-24, 1974, The Metallurgical Society/AIME, pp. 285-300, 1974.

68. Shah, D.C. & Kuhn, H. A.
Application of a Forming Limit Concept to Upsetting and Bolt Heading
Proceedings of ASTM Conference on Compression Testing, March 3-5, 1982.

69. Shenoy, S. P. & Ghosh, C. R.
Continuously Cast Steels for Cold Heading Applications
Tool & Alloy Steels, vol. 17, no. 3, pp. 113-117, 1983.

70. Shewmon, P. G. & Zackay, V. F.
Response of Metals to High Velocity Deformation.
Proceedings of a Technical Conference of the Physical Metallurgical Committee, Estes Park, CO., USA, July 11-12, 1960.

71. Soraya, S.
Maraform - A New Steel Wire For Cold Forming Products
Wire, vol. 38, no. 2, pp. 244-247, March 1988.

72. Tevaarwerk, J. L., Sowerby, R. & Plumtree, A.
The Influence of Prior Cold Working and the Consideration of Die Design on the Cold Headability of 1020 Steel Wire Using an Instrumented Double Blow Heading Machine
Source Book on Cold Forming, ASM, pp. 140-148, 1975.

73. Tozawa, Y., Kato, T. & Kato, N.
Effect of Upsetting Speed on the Upsetting Limit
Annals of the CIRP, vol. 30, no. 1, pp. 203-206, 1981.

74. *The Properties of Materials at High Rates of Strain.*
The Institution of Mechanical Engineers, London, England, 1957.

75. Urtsev, V. N., Maslennikov, V. A., Gubchevskij, V. P., Sarycheva, L. P. & Radyukevich, E. V.
Study of Cracking Resistance of Steel for Cold Heading and Extrusion
Stal', no. 2, pp. 72-73, Feb. 1992.

76. Weidig, C., Rodrigues, P., Espindola, M., Gonzalez, B. & Andrade, M.
Dynamic Stain Aging in Low Carbon Steel Wire Rods
The Wire Association International, Inc. (USA), pp. 83-87, 1994.

77. *What the Designer Should Know About Today's Cold Heading*
Wire, vol. 23, no. 6, pp. 268-270, Nov.-Dec., 1973.

78. Wick, C. H.
Chipless Machining - Methods of Cold Forming Ferrous Metals Including Heading, Rolling, Spinning, Swaging, Extruding & High Energy Rate Forming.
The Industrial Press, New York, New York, 1960.